Performance analysis of adaptive equalization for coherent acoustic communications in the time-varying ocean environment

James C. Preisig[a)]

Department of Applied Ocean Physics and Engineering, Woods Hole Oceanographic Institution, Woods Hole, Massachusetts 02543

Equations are derived for analyzing the performance of channel estimate based equalizers. The performance is characterized in terms of the mean squared soft decision error (σ_s^2) of each equalizer. This error is decomposed into two components. These are the minimum achievable error (σ_o^2) and the excess error (σ_ϵ^2). The former is the soft decision error that would be realized by the equalizer if the filter coefficient calculation were based upon perfect knowledge of the channel impulse response and statistics of the interfering noise field. The latter is the additional soft decision error that is realized due to errors in the estimates of these channel parameters. These expressions accurately predict the equalizer errors observed in the processing of experimental data by a channel estimate based decision feedback equalizer (DFE) and a passive time-reversal equalizer. Further expressions are presented that allow equalizer performance to be predicted given the scattering function of the acoustic channel. The analysis using these expressions yields insights into the features of surface scattering that most significantly impact equalizer performance in shallow water environments and motivates the implementation of a DFE that is robust with respect to channel estimation errors. © *2005 Acoustical Society of America.* [DOI: 10.1121/1.1907106]

I. INTRODUCTION

The use of adaptive coherent equalizers for high rate underwater acoustic communications is increasingly common for a large number of applications. The ability to quantitatively relate the performance of different equalizers to prevailing environmental conditions is important for a number of reasons. First, it allows the relative performance characteristics of different techniques and configurations to be compared and realistic system trade-offs made in the selection and demodulation of demodulation algorithms. Second, it can highlight the factors limiting equalizer performance to guide future research and development efforts. Finally, with the field moving rapidly toward the development of underwater acoustic communications networks using coherent modulation and demodulation techniques, performance predictions as a function of environmental conditions and network topology will be an important input to dynamic network control algorithms.

The paper presents the development and interpretation of quantitative expressions for the performance of three types of channel estimate based adaptive coherent equalizers. Channel estimate based equalizers are those that calculate their filter weights based upon estimates of the time-varying impulse response of the acoustic channel between the transmitter and receiver and the statistics of the ambient noise field. Figure 1 shows the basic structure of channel estimate based equalizers. The three types of equalizers considered here are the channel estimate based decision feedback equalizer (CE-DFE) (Stojanovic *et al.*[1]), the linear MMSE equalizer (L-MMSE), and the passive time-reversal equalizers (P-

TR) (Rouseff *et al.*,[2] Flynn *et al.*[3]). In Stojanovic *et al.*[4] expressions were developed for the total error achieved by a CE-DFE that either has perfect knowledge of the channel impulse response or perfect knowledge of the second-order statistics of the channel impulse response estimation errors.

The expressions developed here are new in that they separately quantify the equalizer errors that are due to the realization of the channel impulse response and the ambient noise and the degradation in performance that is due to the equalizer having imperfect estimates of the channel impulse response. This leads to new insights into the factors that can limit equalizer performance and the characteristics of equalizers that are robust with respect to channel estimation errors. The expressions also allow the performance of the CE-DFE, L-MMSE, and P-TR equalizers to be compared within a common framework when each equalizer has the same information regarding the channel impulse response and the statistics of the ambient noise field. This work is an expansion of the work originally presented in Preisig.[5] This work also presents the results of the processing and analysis of field data collected during the SPACE02 experiment. The SPACE02 experiment was conducted 5 km South of Martha's Vineyard, MA in the Fall of 2002. It focused on investigating the impact of surface processes on high frequency acoustic propagation and communications in shallow water environments.

The organization of this paper is as follows. Section II outlines notation as well as the expressions for the modeled channel impulse response and the equalizer filter coefficients. Similar expressions with varying notations for the filter coefficients of channel estimate based equalizers can be found in Stojanovic *et al.*[4] and standard communications textbooks. Section III presents and discusses the derivation
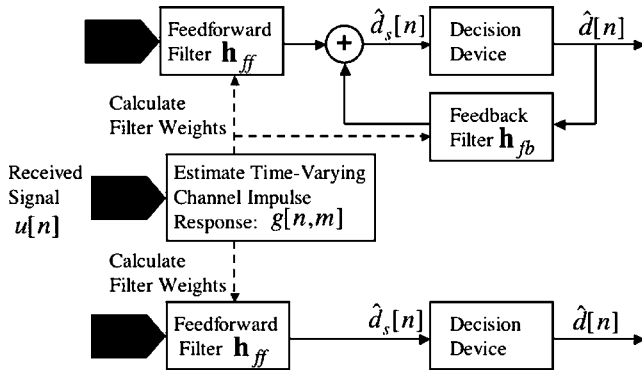

[a)]Electronic mail: jpreisig@whoi.edu

FIG. 1. The structure of channel estimate based coherent equalizers. The received signal, $u[n]$, is processed to generate estimates of the time-varying impulse response of the channel between the transmitter and each receive hydrophone. The impulse response estimates are used to compute the equalizer filter weights. These filter weights are used to implement the equalizer and estimate the desired data symbol. Two different types of equalizers are shown. The upper equalizer is a channel estimate based decision feedback equalizer (CE-DFE) and the lower equalizer is a linear equalizer. The feedforward weights for both filters are denoted here as $\mathbf{h}_{ff}$ and the feedback weights for the CE-DFE are denoted here as $\mathbf{h}_{fb}$. In this paper, two different linear equalizers are considered. The first is the linear minimum mean squared error (L-MMSE) equalizer. The filter weights for this equalizer are denoted in the text as $\mathbf{h}_{lin}$. The second is the passive time-reversal (P-TR) equalizer. The filter weights for this equalizer are denoted in the text as $\mathbf{h}_{tr}$.

of the expressions for the errors achieved by the channel estimate based equalizers given an estimate of the channel impulse response and the statistics of the ambient noise field and channel estimation errors. Section IV describes the algorithm (the exponentially weighted least-squares estimator) used to estimate the channel impulse response and presents a new expression predicting its performance. Section V describes the relevant characteristics of the SPACE02 experiment during which the data analyzed here was collected.

Section VI presents and analyzes the results achieved when processing communications signals from the SPACE02 experiment with CE-DFE and P-TR equalizers. Predictions of equalizer performance using the expressions derived in Secs. III and IV are shown to closely match the observed performance of the equalizers. Two methods of performance prediction are shown. The first method (Sec. VI A) uses estimates of the statistics of the channel estimation error calculated directly from the processed signals. The results of these predictions validate the expressions derived in Sec. III. The second method (Sec. VI B) uses estimates of the statistics of the channel fluctuations to predict the statistics of the channel estimation errors as described in Sec. IV. These predicted statistics of the channel estimation errors are then used to predict equalizer performance. It is this later approach that must ultimately be fully developed to allow equalizer performance to be rigorously related to environmental conditions. Finally, the performance of CE-DFE and P-TR equalizers is compared in Sec. VI C and a CE-DFE with improved robustness with respect to channel estimation errors is presented in Sec. VII. Section VIII presents conclusions of the paper. Derivations of expressions presented in the body of the paper and the method used to estimate channel scattering functions are described in the appendices.

Throughout this paper, boldface uppercase letters denote

matrices, boldface lowercase letters denote vectors (all vectors are assumed to be column vectors), and lowercase letters denote scalar quantities. The superscripts t, $*$, and h denote transpose, complex conjugate, and Hermitian (complex conjugate transpose), respectively. For any square matrix $\mathbf{Q}$, the notation $\tilde{\mathbf{Q}}$ denotes the conjugate symmetric part of $\mathbf{Q}$. That is,

$$\tilde{\mathbf{Q}} \triangleq \frac{\mathbf{Q} + \mathbf{Q}^h}{2}.$$

The symbols $\mathbf{I}$ and $\mathbf{0}$ denote the identity matrix and the matrix or vector of all zeros, respectively. When necessary, the size of the matrices or vectors will be explicitly denoted (e.g., $\mathbf{0}_{N \times M}$ for a matrix of all zeros with N rows and M columns). The caret denotes the estimate of the quantity under the caret (e.g., $\hat{\tilde{\mathbf{g}}}$ denotes the estimate of $\tilde{\mathbf{g}}$).

II. CHANNEL AND EQUALIZER MODEL

All data processing, analysis, and modeling in this paper is done with respect to a sampled baseband received signal. (See Sec. V for a description of this baseband signal.) Thus all discussion is with respect to discrete time signals and processes. The acoustic channel is modeled as a time-varying, discrete time system described by the complex baseband time-varying impulse response. (See Proakis[6] and Van Trees[7]). The received signal at time n is given by

$$u[n] = \sum_{m=-N_a}^{N_c-1} g^*[n,m] d[n-m] + v[n], \qquad (1)$$

where $g[n,m]$ is the baseband complex time-varying impulse response relating the input signal at time $(n-m)$ to the output signal at time n, $d[n]$ is the complex baseband transmitted data, and $v[n]$ is complex baseband observation noise. The quantities N_a and N_c denote, respectively, the number of acausal and causal taps in the impulse response.[8] This equation can be put into the vector form of

$$u[n] = \tilde{\mathbf{g}}^h[n] \tilde{\mathbf{d}}[n] + v[n]. \qquad (2)$$

where

$$\tilde{\mathbf{g}}[n] \triangleq [g[n,N_c-1],\ldots,g[n,0],\ldots,g[n,-N_a]]^t,$$

and

$$\tilde{\mathbf{d}}[n] \triangleq [d[n-N_c+1],\ldots,d[n],\ldots,d[n+N_a]]^t$$

are samples of the impulse response and transmitted data symbols, respectively. In this section, the received signal is assumed to be sampled at the transmit symbol rate. The extension of the analysis to fractionally spaced systems is conceptually straightforward, but the notation is cumbersome. The final results of the analysis are equally applicable to symbol rate and fractionally spaced systems. Note that the experimental data presented in this paper were fractionally sampled at a rate of 2 samples/symbol (See Sec. V).

The equalizers considered here (Fig. 1) each consist of a linear, finite impulse response (FIR) feedforward filter that filters the received signals and, in the case of the CE-DFE, a FIR feedback filter that filters and feeds back estimates of the transmitted data symbol. The output of the filter is the soft

James C. Preisig: Robust coherent equalization and performance analysis

decision estimate, $\hat{d}_s[n]$, of the transmitted data symbol, $d[n]$. The estimate $\hat{d}_s[n]$ is the input to a decision device that generates the final estimate, $\hat{d}[n]$, of the transmitted data symbol.

For a linear equalizer (e.g., the L-MMSE and P-TR equalizers) the soft decision estimate of the transmitted data symbol, $\hat{d}_s$, is given by

$$\hat{d}_s[n] = \mathbf{h}^h[n]\mathbf{u}[n], \qquad (3)$$

where $\mathbf{h}[n]$ is a vector of the feedforward filter coefficients at time n and

$$\mathbf{u}[n] \triangleq [u[n-L_c+1],\ldots,u[n],\ldots,u[n+L_a]]^t. \qquad (4)$$

Here, L_c and L_a denote the number of causal and acausal taps, respectively, of the feedforward filter. The notation $\mathbf{h}_{\text{lin}}$ and $\mathbf{h}_{\text{tr}}$ will be used to denote the filter coefficient vectors for the L-MMSE and P-TR equalizers, respectively. For the CE-DFE, $\hat{d}_s$ is given by

$$\hat{d}_s[n] = \mathbf{h}_{\text{ff}}^h[n]\mathbf{u}[n] + \mathbf{h}_{\text{fb}}^h[n]\hat{\mathbf{d}}_{\text{fb}}[n]. \qquad (5)$$

Here, $\mathbf{h}_{\text{ff}}$ and $\mathbf{h}_{\text{fb}}$ are vectors of the coefficients of the CE-DFE feedforward and feedback filters, respectively. For a feedback filter of length L_{fb} symbols, $\hat{\mathbf{d}}[n]$ is a vector of estimates of past transmitted data symbols given by $\hat{\mathbf{d}}_{fb}[n] \triangleq [\hat{d}[n-L_{fb}],\ldots,\hat{d}[n-1]]^t$. The span of the feedback filter should be less than or equal to the causal delay spread of the convolution of the channel impulse response and the feedforward filter. Therefore, $L_{\text{fb}} \le L_c + N_c - 2.$[9]

Combining Eqs. (2) and (4) yields

$$\mathbf{u}[n] = \mathbf{G}[n]\mathbf{d}[n] + \mathbf{v}[n], \qquad (6)$$

where

$$\mathbf{d}[n] \triangleq [d[n-L_c-N_c+2],\ldots,d[n],\ldots,d[n+L_a+N_a]]^t$$

and

$$\mathbf{v}[n] \triangleq [v[n-L_c+1],\ldots,v[n],\ldots,v[n+L_a]]^t.$$

$\mathbf{G}[n]$ is the channel impulse response matrix with the ith row composed of $\tilde{\mathbf{g}}^h[n-L_c+i]$ packed with leading and trailing zeros to position it in the appropriate columns of the matrix with respect to the elements of the vector $\mathbf{d}[n]$.

The notation presented thus far has been specific to single channel equalizers. Multichannel equalizers are accommodated within this notation by stacking the feedforward filter coefficient vector for each channel into a single larger vector, stacking the received signal vector, $\mathbf{u}$, for each channel into a single larger vector, and stacking the impulse response matrix, $\mathbf{G}$, for each channel into a single matrix with the same number of columns as the original matrix but a greater number of rows.

It is instructive to represent $\mathbf{G}$ using its column vectors indexed in the following manner:

$$\mathbf{G}[n] = [\mathbf{g}_{(N_c+L_c-2)},\ldots,\mathbf{g}_1,\mathbf{g}_0,\mathbf{g}_{-1},\ldots,\mathbf{g}_{-(N_a+L_a)}], \qquad (7)$$

The dependence of the columns of $\mathbf{G}[n]$ on the time index n will now be suppressed for notational convenience. Note that the rows of $\mathbf{G}$ are composed of the appropriately positioned versions of the impulse response vector $\tilde{\mathbf{g}}^h$. In this way, each row of $\mathbf{G}$ relates a subset of the elements of the transmitted data vector $\mathbf{d}[n]$ to the corresponding element of the received signal vector $\mathbf{u}[n]$. In contrast, the vector $\mathbf{g}_i$ denoting a particular column of $\mathbf{G}$ is a replica vector for the data symbol $d[n-i]$ in the received signal vector $\mathbf{u}[n]$. That is, it specifies the contribution of one transmitted data symbol symbol $d[n-i]$ to the entire received signal vector.

Partition the transmit data symbols in $\mathbf{d}[n]$ into three groups: $\mathbf{d}_{\text{fb}}[n] \triangleq [d[n-L_{\text{fb}}],\ldots,d[n-1]]^t$, $d[n]$, and $\mathbf{d}_o[n]$ which is composed of the remaining elements of $\mathbf{d}[n]$. Partition the columns of $\mathbf{G}[n]$ into three similarly defined sets: $\mathbf{G}_{\text{fb}}$, $\mathbf{g}_0$, and $\mathbf{G}_o$. Then Eq. (6) can be rewritten as

$$\mathbf{u}[n] = \mathbf{g}_0 d[n] + \mathbf{G}_{\text{fb}}\mathbf{d}_{\text{fb}}[n] + (\mathbf{v}[n] + \mathbf{G}_o\mathbf{d}_o[n]). \qquad (8)$$

The first term is the portion of the received signal vector, $\mathbf{u}[n]$, that corresponds to the transmitted data symbol to be estimated, $d[n]$. The second term is the portion of $\mathbf{u}[n]$ that can be canceled by the output of the feedback filter in a CE-DFE, and the terms in the parentheses represent an effective observation noise that the feedforward filter must try to eliminate. Assuming that the data sequence is a zero-mean, white sequence with a variance of one,[10] the data sequence is independent of the channel impulse response and $v[n]$, and that $\mathbf{v}[n]$ is a zero-mean sequence with covariance $\mathbf{R}_v$ that is independent of the channel impulse response, the effective noise correlation matrix, $\mathbf{Q}$, can be written as

$$\mathbf{Q} = \mathbf{R}_v + \mathbf{G}_o\mathbf{G}_o^h. \qquad (9)$$

With the model and quantities so defined, a number of approaches can be used to calculate the optimal filter coefficients. One such approach is given in Stojanovic *et al.*[4] In that paper, the effective noise correlation matrix, denoted with the symbol $\mathbf{R}$, includes the impact of channel estimation errors. Therefore, the calculated filter coefficients and subsequent error analysis are valid for the case where the DFE has accurate knowledge of both the noise statistics and the second-order statistics of the channel estimation errors. For the filter calculation and performance analysis presented here, there is no assumption that the DFE knows the statistics of the channel estimation errors.

The filter coefficients for the three equalizers are calculated using estimated quantities for $\mathbf{R}_v$, $\mathbf{G}$, and therefore $\mathbf{Q}$. In the following expressions, these estimated quantities are denoted by the caret (e.g., $\hat{\mathbf{R}}_v$). The filter coefficient vectors for the L-MMSE and CE-DFE equalizers are selected to minimize the mean squared soft decision error ($\mathrm{E}[|\hat{d}_s[n] - d[n]|^2]$) assuming that the estimates of $\mathbf{R}_v$ and $\mathbf{G}$ are accurate and that the statistical assumptions stated in the paragraph before Eq. (9) hold. The expressions for these filter coefficient vectors are

$$\mathbf{h}_{\text{ff}} = \frac{\hat{\mathbf{Q}}^{-1}\hat{\mathbf{g}}_0}{1 + \hat{\mathbf{g}}_0^h\hat{\mathbf{Q}}^{-1}\hat{\mathbf{g}}_0}, \qquad \mathbf{h}_{\text{fb}} = -\hat{\mathbf{G}}_{\text{fb}}^h\mathbf{h}_{\text{ff}}, \qquad (10)$$

$$\mathbf{h}_{\text{lin}} = \frac{(\hat{\mathbf{Q}} + \hat{\mathbf{G}}_{\text{fb}}\hat{\mathbf{G}}_{\text{fb}}^h)^{-1}\hat{\mathbf{g}}_0}{1 + \hat{\mathbf{g}}_0^h(\hat{\mathbf{Q}} + \hat{\mathbf{G}}_{\text{fb}}\hat{\mathbf{G}}_{\text{fb}}^h)^{-1}\hat{\mathbf{g}}_0}. \qquad (11)$$

The P-TR equalizer is a normalized matched filter so its coefficients are given by

$$\mathbf{h}_{\text{tr}} = \frac{\hat{\mathbf{g}}_0}{\hat{\mathbf{g}}_0^h \hat{\mathbf{g}}_0}. \tag{12}$$

See Appendix A for a derivation of Eqs. (10)–(12).

III. EQUALIZER PERFORMANCE PREDICTIONS

Here, equalizer performance is characterized in terms of the variance of the soft decision error $\epsilon_s = (\hat{d}_s[n] - d[n])$. This error will depend on both the estimate of the channel impulse response as well as the error in this estimate. For the analytical results presented here, it is assumed that correct values of the transmitted signal are used to estimate the channel impulse response and as the input to the feedback filter of the CE-DFE. The experimental data were processed in this same manner. That is, the equalizers were run in a "training mode." The impact of the decay in the quality of the channel estimate resulting from using incorrect signal decisions in the estimation algorithm or the feedback of incorrect signal decisions has not been treated here. Thus, the observed and predicted values of the variance of the soft decision error are lower bounds on what could actually be achieved.

Let the true channel impulse response matrix be given by

$$\mathbf{G}[n] = \hat{\mathbf{G}}[n] + \mathbf{E}_G, \tag{13}$$

where $\mathbf{E}_G$ is the error in the estimate of the channel impulse response matrix. Then for the CE-DFE, combining Eqs. (5) and (8) results in

$$\hat{d}_s[n] = \mathbf{h}_{\text{ff}}^h[n](\mathbf{g}_0 d[n] + \mathbf{G}_{\text{fb}} \mathbf{d}_{\text{fb}}[n] + \mathbf{v}[n] + \mathbf{G}_o \mathbf{d}_o[n])$$
$$+ \mathbf{h}_{\text{fb}}^h[n] \hat{\mathbf{d}}_{\text{fb}}[n].$$

Then, substituting in Eqs. (10) and (13), the soft decision estimate can be written as

$$\hat{d}_s[n] = \mathbf{h}_{\text{ff}}^h[n](\hat{\mathbf{g}}_0 d[n] + \mathbf{v}[n] + \hat{\mathbf{G}}_o \mathbf{d}_o[n]) + \mathbf{h}_{\text{ff}}^h[n]$$
$$\times (\hat{\mathbf{G}}_{\text{fb}} \mathbf{d}_{\text{fb}}[n] - \hat{\mathbf{G}}_{\text{fb}} \hat{\mathbf{d}}_{\text{fb}}[n]) + \mathbf{h}_{\text{ff}}^h[n] \mathbf{E}_G \mathbf{d}[n].$$

Assuming that the past symbol decisions that are inputs to the feedback filter are accurate, the second term equals zero and this becomes

$$\hat{d}_s[n] = \mathbf{h}_{\text{ff}}^h[n](\hat{\mathbf{g}}_0 d[n] + \mathbf{v}[n] + \hat{\mathbf{G}}_o \mathbf{d}_o[n])$$
$$+ \mathbf{h}_{\text{ff}}^h[n] \mathbf{E}_G \mathbf{d}[n]. \tag{14}$$

Subtracting $d[n]$ from both sides of Eq. (14) yields the following expression for the soft decision error of a CE-DFE:

$$\epsilon_s[n] = (\mathbf{h}_{\text{ff}}^h[n](\hat{\mathbf{g}}_0 d[n] + \mathbf{v}[n] + \hat{\mathbf{G}}_o \mathbf{d}_o[n]) - d[n])$$
$$+ \mathbf{h}_{\text{ff}}^h[n] \mathbf{E}_G \mathbf{d}[n]. \tag{15}$$

Similarly, the expression for the soft decision estimate for L-MMSE and P-TR equalizers can be written as

$$\hat{d}_s[n] = \mathbf{h}^h[n](\hat{\mathbf{g}}_0 d[n] + \mathbf{v}[n] + \hat{\mathbf{G}}_o \mathbf{d}_o[n] + \hat{\mathbf{G}}_{\text{fb}} \mathbf{d}_{\text{fb}}[n])$$
$$+ \mathbf{h}^h[n] \mathbf{E}_G \mathbf{d}[n], \tag{16}$$

where $\mathbf{h}[n]$ is the appropriate filter coefficient vector ($\mathbf{h}_{\text{lin}}[n]$ or $\mathbf{h}_{\text{tr}}[n]$). Subtracting $d[n]$ from both sides of Eq. (16) yields the following expression for the soft decision error of the L-MMSE and P-TR equalizers:

$$\epsilon_s[n] = (\mathbf{h}^h[n](\hat{\mathbf{g}}_0 d[n] + \mathbf{v}[n] + \hat{\mathbf{G}}_o \mathbf{d}_o[n] + \hat{\mathbf{G}}_{\text{fb}} \mathbf{d}_{\text{fb}}[n])$$
$$- d[n]) + \mathbf{h}^h[n] \mathbf{E}_G \mathbf{d}[n]. \tag{17}$$

Under the assumption that the estimate of the channel impulse response is a minimum mean squared error estimate, the error matrix $\mathbf{E}_G$ is uncorrelated with the estimated channel impulse response matrix and the received signal and the expectation of $\mathbf{E}_G$ conditioned on $\hat{\mathbf{G}}$ equals zero. Under these conditions, the first and second terms in these expressions are uncorrelated. The variance of the first term represents the minimum achievable error (MAE) of the equalizer and is denoted by σ_o^2. This is the error that will be achieved by the equalizer given that it has perfect estimates of the channel impulse response and the noise statistics. This error depends on the static structure of the channel impulse response and the statistics of the ambient noise but not on the dynamics of the channel impulse response fluctuations. The variance of the second term is the excess error and is denoted by σ_ϵ^2. This error is the additional soft decision error that is due to errors in estimating the channel impulse response. The variance of the soft decision error is given by $\sigma_s^2 = \sigma_o^2 + \sigma_\epsilon^2$.

The MAE can be calculated by substituting the appropriate expressions for the equalizer coefficients into the first term in Eqs. (15) and (17) and calculating the variance of the resulting term. For the three different equalizers, the variance of the MAE is given by

$$\sigma_{o_{\text{DFE}}}^2 = \frac{1}{1 + \hat{\mathbf{g}}_0^h \hat{\mathbf{Q}}^{-1} \hat{\mathbf{g}}_0}, \tag{18}$$

$$\sigma_{o_{\text{lin}}}^2 = \frac{1}{1 + \hat{\mathbf{g}}_0^h (\hat{\mathbf{Q}} + \hat{\mathbf{G}}_{\text{fb}} \hat{\mathbf{G}}_{\text{fb}}^h)^{-1} \hat{\mathbf{g}}_0}, \tag{19}$$

$$\sigma_{o_{\text{tr}}}^2 = \frac{\hat{\mathbf{g}}_0^h (\hat{\mathbf{Q}} + \hat{\mathbf{G}}_{\text{fb}} \hat{\mathbf{G}}_{\text{fb}}^h) \hat{\mathbf{g}}_0}{(\hat{\mathbf{g}}_0^h \hat{\mathbf{g}}_0)^2}. \tag{20}$$

See Appendix A for a derivation of these expressions for the variance of the MAE for each type of equalizer.

Comparing Eqs. (18), (19), and (20), it can be shown that

$$\sigma_{o_{\text{DFE}}}^2 \leq \sigma_{o_{\text{lin}}}^2 \leq \sigma_{o_{\text{tr}}}^2.$$

Furthermore, it can be shown that $\sigma_{o_{\text{DFE}}}^2$ and $\sigma_{o_{\text{lin}}}^2$ will always decrease when the number of received signal channels or the length of the feedforward of feedback filters is increased.

The reduction in MAE when comparing the MAE of the L-MMSE equalizer to the P-TR equalizer is due to the MMSE adaptation of the former equalizer while the reduction in MAE when comparing the CE-DFE to the L-MMSE equalizer is due to the cancellation of the interference energy associated with the "replica vectors" corresponding to the columns of $\mathbf{G}_{\text{fb}}$. For all three equalizers, the MAE can be evaluated in terms of the quadratic product of the replica vector associated with the data symbol being estimated, $\mathbf{g}_0$,

and a matrix determined by the observation noise and the outer product of a subset of the columns of $\mathbf{G}$ ($\mathbf{G}_o$ for the CE-DFE, $\mathbf{G}_o$ and $\mathbf{G}_{fb}$ for the L-MMSE and P-TR equalizers) that are the replica vectors of interfering data symbols. The structure of the channel impulse response matrix impacts the minimal achievable error through these replica vectors.

The variance of the excess error is the variance of the second term in Eqs. (15) and (17). For the three different equalizers, this yields a common form of

$$\sigma^2_{\epsilon_{\text{DFE}}} = \mathbf{h}^h_{\text{ff}} \mathbf{R}_{E_G} \mathbf{h}_{\text{ff}}, \tag{21}$$

$$\sigma^2_{\epsilon_{\text{lin}}} = \mathbf{h}^h_{\text{lin}} \mathbf{R}_{E_G} \mathbf{h}_{\text{lin}}, \tag{22}$$

$$\sigma^2_{\epsilon_{\text{tr}}} = \mathbf{h}^h_{\text{tr}} \mathbf{R}_{E_G} \mathbf{h}_{\text{tr}}, \tag{23}$$

where $\mathbf{R}_{E_G} \triangleq \mathrm{E}[\mathbf{E}_G \mathbf{E}^h_G | \hat{\mathbf{G}}]$. Thus the sensitivity of each equalizer to channel impulse response estimation errors is determined by the magnitude squared of the vector of the equalizer's feedforward filter coefficients and the projection of these coefficient vectors on the eigen-structure of $\mathbf{R}_{E_G}$. In the special case where $\mathbf{R}_{E_G}$ is a scalar times the identity matrix, the sensitivity of each equalizer to channel estimation errors is proportional to the magnitude squared of the feedforward filter weight vector.

The soft decision error expressions derived in this section and used in Sec. VI B assume that the statistics of the channel and data estimation errors are conditioned upon the channel estimate. Thus, the channel estimate is considered to be a deterministic quantity and the actual channel realization a stochastic quantity. This approach is taken for several reasons. First, it yields results that offer better insight into the functional dependence of equalizer performance on the deterministic channel structure and the rate of fluctuation of the channel impulse response than do methods that condition the statistics on the true channel state. Second, unconditional statistics (i.e., conditioned on neither the channel impulse response nor the estimate of the channel impulse response) would not clearly highlight some aspects of the relationship between important physical processes and the performance of the algorithms considered here. An example of such a relationship is the cyclic nature of the soft decision error and the relationship of the time scale of the fluctuation to the dominant surface wave period discussed in Sec. VI A. Third, the expressions presented here can be used to aid in the optimal dynamic configuration of channel estimate based equalizers given channel estimates and estimates of the channel dynamics. In this case, these conditional statistics would be the appropriate ones to use. Finally, the experimental results presented here indicate that the resulting expressions yield results that are relatively accurate to within the limits of our ability to predict the correlation matrix $\mathbf{R}_{E_G}$.

IV. CHANNEL ESTIMATION AND ERROR

The excess error exhibited by any channel estimate based equalizer depends upon the quality of the channel estimate. For the analysis and results presented here, the channel estimation algorithm is the exponentially weighted least squares algorithm. While this algorithm does not yield mini-mum mean squared error estimates of the channel impulse response and therefore results in a violation of the assumption that the channel esimates and estimation error are uncorrelated, the analysis of experimental data in Sec. VI indicates that the assumption is sufficiently valid for the prediction of excess error.

With the exponentially weighted least squares algorithm, the estimate of the channel impulse response is given by

$$\hat{\tilde{\mathbf{g}}}[n] = \arg \min_{\tilde{\mathbf{g}}} \sum_{m=0}^{n} \lambda^{n-m} |u[m] - \tilde{\mathbf{g}}^h \tilde{\mathbf{d}}[m]|^2, \tag{24}$$

where λ is a constant "forgetting factor" between zero and one. Assume that the channel impulse response, $\tilde{\mathbf{g}}[n]$, is a zero-mean, wide-sense stationary random process with correlation matrix $\mathbf{R}_{\tilde{\mathbf{g}},\tilde{\mathbf{g}}}[m] \triangleq \mathrm{E}[\tilde{\mathbf{g}}[n]\tilde{\mathbf{g}}^h[n+m]]$. Then, the error correlation matrix $\mathbf{R}_{\epsilon,\epsilon}[1] \triangleq \mathrm{E}[(\hat{\tilde{\mathbf{g}}}[n] - \tilde{\mathbf{g}}[n+1])(\hat{\tilde{\mathbf{g}}}[n] - \tilde{\mathbf{g}}[n+1])^h]$ is given by

$$\mathbf{R}_{\epsilon,\epsilon}[1] = \frac{1}{2\pi} \int_{-\pi}^{\pi} \frac{|e^{-j\omega} - 1|^2}{|1 - \lambda e^{-j\omega}|^2} \mathbf{S}_{\tilde{\mathbf{g}},\tilde{\mathbf{g}}}(\omega) d\omega$$
$$+ \frac{(1-\lambda)}{(1+\lambda)} \sigma^2_v \mathbf{I}, \tag{25}$$

where

$$\mathbf{S}_{g,g}(\omega) = \sum_{m=-\infty}^{\infty} \mathbf{R}_{\tilde{\mathbf{g}},\tilde{\mathbf{g}}}[m] e^{-j\omega m} \tag{26}$$

is the spectral correlation matrix for the time-varying channel impulse response vector $\tilde{\mathbf{g}}[n]$. Here, the observation noise correlation matrix $\mathbf{R}_v$ is assumed to equal $\sigma^2_v \mathbf{I}$ and the data symbol variance is assumed equal to one as stated previously. The first term in Eq. (25) is the lag error resulting from the time variation of the channel while the second term is the error variance due to the observation noise. See Appendix B for a derivation of Eq. (25). While experimental data will show that the channel does not exhibit the behavior of a stationary random process, this model is useful for predicting the algorithm dependence on channel behavior over short time periods.

Note that the total mean squared channel estimation error equals the trace of the error correlation matrix. Thus, it is the diagonal elements of this matrix that determine the total mean squared estimation error, and through Eq. (25), this depends on the diagonal elements of the spectral correlation matrix. These diagonal elements are the channel scattering function (See Proakis[6] and Van Trees[7]) defined as a function of delay and Doppler. Figure 2 shows schematically the calculation of the first term in Eq. (25) from the channel scattering function.

The error correlation matrix $\mathbf{R}_{E_G}$ required for the calculation of σ^2_ϵ is related to the error correlation matrix $\mathbf{R}_{\epsilon,\epsilon}[1]$ defined in Eq. (25). The matrix is reasonably approximated by a Toeplitz matrix with each element of the ith diagonal of $\mathbf{R}_{E_G}$ equal to the sum of the elements along the ith diagonal of $\mathbf{R}_{\epsilon,\epsilon}[1]$. That is, the terms on the ith diagonal of $\mathbf{R}_{E_G}$ represent the sum of the correlations between the error in estimating all pairs of taps of the channel impulse response
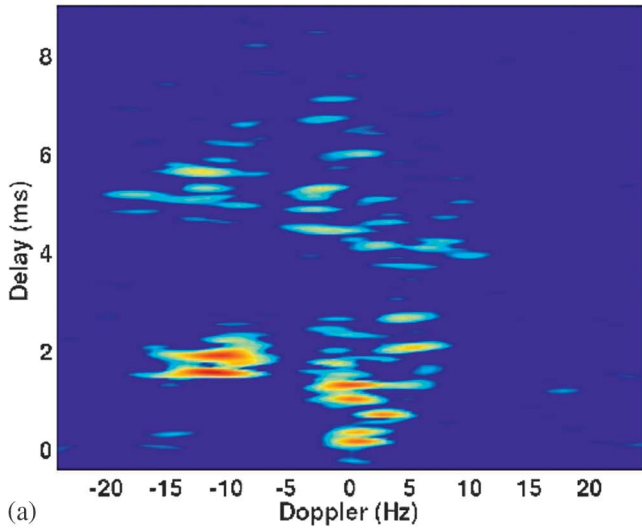
(a)
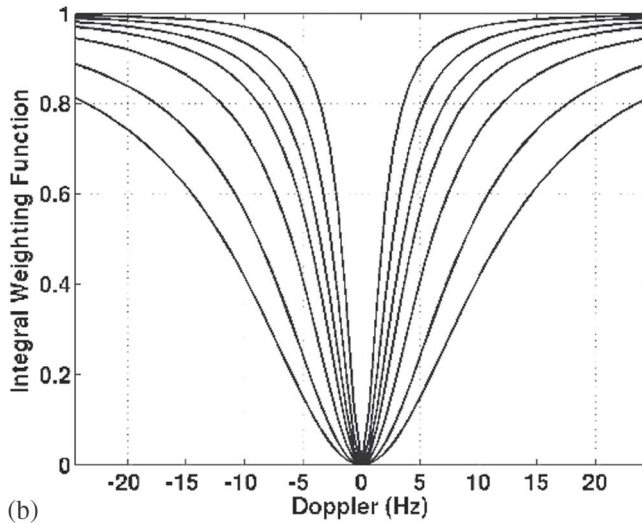
(b)

FIG. 2. Graphic representation of the use of a scattering function to predict the lag error [i.e., the first term in Eq. (25)] that is achieved by an exponentially weighted least-squares algorithm used in estimating the time-varying channel impulse response. (a) An estimated scattering function of the channel encountered during the SPACE02 experiment. See Sec. V and Appendix C for descriptions of the experiment and the method used to estimate the scattering function, respectively. This panel is shown in log scale and the range of the color scale is 16 dB. The delay axis is shifted so that a delay of zero corresponds to the peak of the direct path arrival. For each delay tap of the sampled impulse response (the vertical axis on the upper panel), the lag error associated with estimating that tap is a weighted integral across Doppler of the scattering function evaluated at that delay. (b) The weighting function for different values of the exponential weighting factor λ. The bottom curve corresponds to the lowest value of λ (λ=0.9933) with successively higher curves corresponding to successively higher values of λ. The top curve corresponds to a value of λ=0.999. For this figure, a least-squares algorithm update rate of 11.16 kHz is assumed. Note that as λ increases thus increasing the "averaging interval" of the least-squares estimation algorithm, the weighting which determines the contribution of energy at each Doppler frequency to the estimation error increases. Thus, energy at low Doppler frequencies that has an insignificant contribution to the estimation error at low values of λ can make a significant contribution to the estimation error at the highest values of λ.

separated by a delay of i samples. For wide-sense stationary, uncorrelated scattering (WSSUS) channels, $\mathbf{R}_{\epsilon,\epsilon}[1]$ is a diagonal matrix thus resulting in $\mathbf{R}_{E_G}$ equaling the trace of $\mathbf{R}_{\epsilon,\epsilon}[1]$ times the identity matrix. Therefore, evaluation of Eqs. (21)–(23) for this case shows that the excess error for
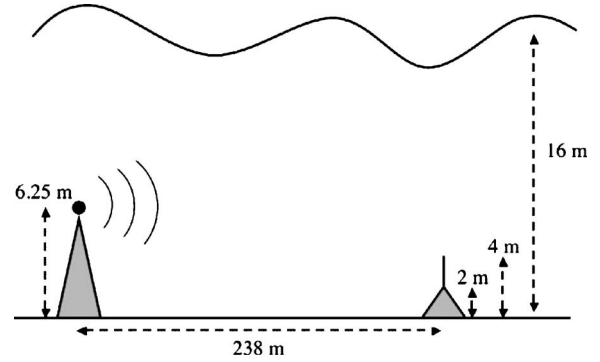

FIG. 3. Side view of the SPACE02 experiment. A source transducer was mounted 6.25 m above the bottom on top of a rigid tripod. The transducer was spherical and had an omni-directional beampattern. A receive hydrophone array was mounted on top of a rigid tripod that was 2 m tall. This vertical, linear array consisted of eight hydrophones with variable spacing and a total aperture of 2.1 m. Data presented in this paper were collected on the center four hydrophones of the array. The spacing between these hydrophones (from bottom to top) was 6.4, 3.7, and 8.4 cm yielding a total aperture of 18.5 cm. The lowermost of the hydrophones was 2.7 m above the bottom. In all cases where results are shown from processing data from just one hydrophone, the hydrophone used is the lowermost of the four. The horizontal range from the transducer to the hydrophone array was 238 m. The bottom was flat in the area of the experiment. The water depth was approximately 16 m during the experiment.

each equalizer equals the trace of $\mathbf{R}_{\epsilon,\epsilon}[1]$ times the magnitude squared of the feedforward filter coefficient vector for each equalizer. Furthermore, for the case of the WSSUS channel the matrix $\mathbf{R}_{E_G}$ can be completely determined from the scattering function of the channel.

This result is independent of the distribution of the channel estimation error among the taps of the channel impulse response vector. While these correlation matrices are not conditioned upon the channel estimate (or equivalently, the calculated feedforward filter weights) as required to properly evaluate Eqs. (21)–(23), they do lend insights into the channel and equalizer characteristics that impact robustness with respect to channel estimation errors. Analysis of data in Sec. VI indicates that in some cases the uncorrelated scattering assumption is sufficiently valid to allow for accurate prediction of the excess error and in other cases the full correlation matrix $\mathbf{R}_{E_G}$ is needed.

V. THE SPACE02 EXPERIMENT

The experimental data presented in this paper were collected during the Surface Processes and Acoustic Communications Experiment (SPACE02) that took place at the Air Sea Interaction Tower of the Martha's Vineyard Coastal Observatory in the Fall of 2002. A side view of the relevant portion of the experiment and associated physical parameters are shown in Fig. 3. A reference hydrophone was deployed at the same depth as and approximately 1 m from the source transducer to monitor signal transmissions. The sound speed during the experiment was estimated to be approximately 1485 m/s during the time that the data were collected. The signal transmission and data acquisition systems were both driven by a common sampling clock resulting in no clock drift between the two systems. This enabled reliable and precise timing of signal transmissions and receptions. Thus, given

the fact that the source transducer and receive hydrophones were deployed on rigid tripods, all fluctuations or drifts in the received signal relative to the transmitted signal can be attributed to environmental fluctuations.

The transmit and receive signals were sampled at a rate of 44.6428 kHz. Transmit signals were generated with a center frequency of 14 kHz, and were prefiltered to provide an approximately flat system frequency response over a bandwidth of approximately 12 kHz. The signals were transmitted at 56 s intervals with approximately 53.2 s of continuous transmission during each interval. The data presented here are from transmissions of a binary phase shift keyed signal modulated by continuous repetitions of a 4095 point maximum length shift register sequence (m-seq) (see Proakis[6]). The symbol rate of these data was 11160.7 symbols/s. The received signals were modulated to baseband, low pass filtered, and downsampled by a factor of 2 to yield a baseband sample rate of 22.3214 kHz or 2 samples per symbol. This baseband signal was the input to subsequent channel estimation, scattering function estimation, and equalization algorithms.

Data processed here were collected during two different 56 s transmission intervals. The data sets from these two intervals will be referred to as data set 331 and data set 334. The main difference between the two intervals is that significant wave height during the interval corresponding to data set 331 was 0.3 m (very calm conditions) while the significant wave height during the interval corresponding to data set 334 was 3.0 m (very rough conditions). Channel impulse response estimates made using these data are shown in Fig. 4.

VI. EQUALIZER PERFORMANCE ANALYSIS

The data from the SPACE02 experiment was processed using CE-DFE and P-TR equalizers to compare observed and predicted performance. As described previously, the equalizers were run in ''training'' mode. That is, the channel estimation algorithm was given perfect estimates of the transmitted data with which to estimate the channel impulse response. In addition, the data symbols fed back through the feedback filter of the CE-DFE were the true data symbols rather than the estimated data symbols. Note that in channel estimate equalizers, the most up-to-date channel estimate available for calculating filter weights would be the one that could be estimated using data symbols that were demodulated up to that time. This lag between the channel estimate and the data symbols being estimated by the equalizer was enforced in all processing.

In all cases, the length of the impulse response estimate was 175 symbols (350 baseband samples) corresponding to a delay spread of 15.7 ms. The channel estimation algorithm used exponential weighting factors of $\lambda=0.9966$ and $\lambda=0.9933$, respectively, for data sets 331 and 334. The algorithms updated estimates at the symbol rate yielding effective averaging intervals, defined as $1/(1-\lambda)$, of 294 and 149 symbols, respectively. This channel length and these exponential weighting factors offered the best compromise between tracking enough of the channel impulse response to account for the total energy in the received signal and keeping the
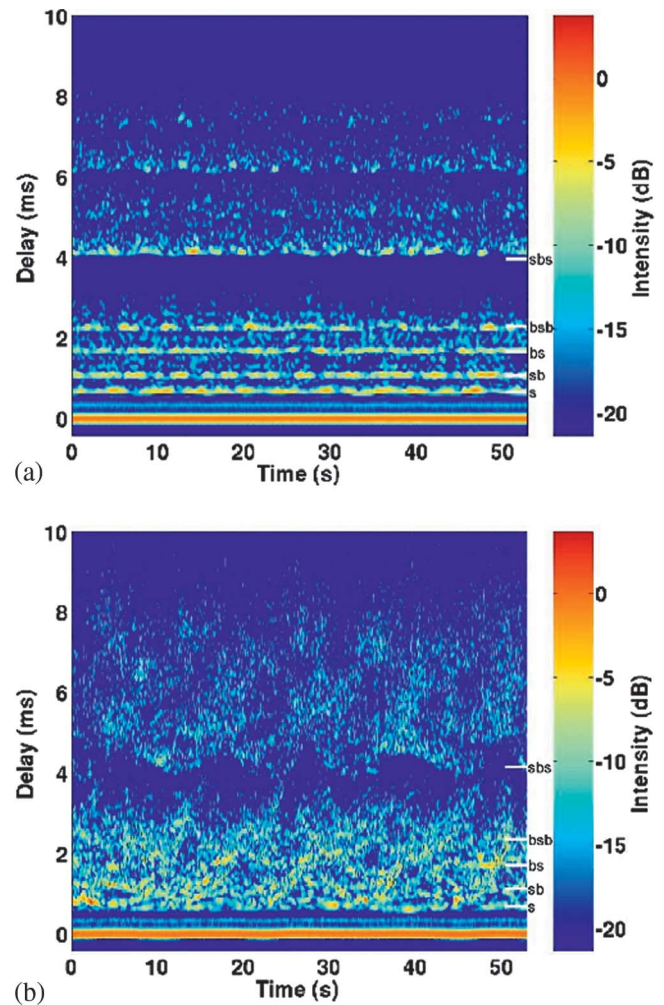

FIG. 4. Intensity of the estimates of the time-varying impulse response of the channel between the transducer and the lowermost of the hydrophones from which data is presented. The estimates were made using exponentially weighted least-squares algorithms. These estimates use data from two different 53.2 s transmission sequences. (a) The estimates made using data collected during a period when the significant wave height was 0.3 m. This is referred to in the paper as data set 331. (b) The estimates made using data collected during a period when the significant wave height was 3.0 m. This is referred to in this paper as data set 334. In (a) and (b), the levels are represented in dB relative to the mean intensity of the direct path arrival during the period. The delay axis has been shifted so that a delay of zero corresponds to the peak of the direct path arrival. The direct and first bottom bounce arrivals make up the thick solid orange line at the bottom of (a) and (b). The white tic marks at the right edge of (a) and (b) represent the predicted arrival time of each successive arrival as labeled on the right-hand side. In order from bottom to top these are the surface, surface/bottom, bottom surface, bottom/surface/bottom, and surface/bottom/surface arrivals. The estimates shown in (a) show a stable arrival pattern and close agreement between predicted and actual arrival times. The estimates in (b) show a highly variable arrival pattern. The arrival time predictions were made assuming two-dimensional propagation in the vertical plane joining the source and receiver and assuming a flat sea surface and bottom. Deviations from this assumption for an arrival due to scattering from a location other than the nominal specular reflection point will almost always result in a greater delay of the arrival (the one exception is the scattering from the trough of a wave at which the sea surface is below the assumed sea surface level). Thus, the predicted arrival times represent the earliest expected arrival time for a particular path. While the estimates in (b) do not line up with the predicted arrival times, the data and the predicted arrival times for the surface and surface/bottom/surface arrivals support this interpretation and represent the earliest arrival times for the single and double surface bounce arrivals, respectively.

estimated channel length small enough to enable tracking of rapid channel fluctuations. The lower value of λ for processing data set 334 was required to enable better tracking of the rapid channel fluctuations. The ability of this trade-off to enable improved overall performance was due in part to the very high signal-to-noise ratio (SNR) of the data set.

The observed SNR was 41 dB. However, the cut off of the estimated impulse response at a delay spread of 15.7 ms resulted in some late arriving energy due to the tail of the channel impulse response appearing as ambient noise from the perspective of the channel estimation and equalization algorithms. When accounting for this energy as part of the ambient noise, the effective SNR dropped to 18.7 dB. In calculating the CE-DFE coefficients, it was assumed that the ambient noise correlation matrix had the form of $\mathbf{R}_v = \sigma_v^2 \mathbf{I}$, where σ_v^2 was based upon either the observed ambient noise level or the observed ambient noise level plus the late arriving energy from the tail of the channel impulse response. These two values are denoted as σ_{va}^2 and σ_{vt}^2, respectively. For the fractionally spaced equalizer used here, the sampled ambient noise is not white because the downsampling filter limits its bandwidth to approximately one half of the full 2π rad/sample of available bandwidth. Thus the model of $\mathbf{R}_v = \sigma_v^2 \mathbf{I}$ is not valid in the MAE expressions. However, at the SNRs observed here, this inaccuracy in the ambient noise model is not expected to significantly affect the results.

The prediction of equalizer performance required estimating both the MAE and the excess error. The excess error calculations required estimates of the error correlation matrix, $\mathbf{R}_{E_G}$. These estimates were made using two different methods. The first was to calculate a running average of the correlation matrix of the residual prediction error of the input signal to the feedforward equalizer. That is

$$\mathbf{e}_{\text{ff}}[n] = \mathbf{u}[n] - \hat{\mathbf{u}}[n] = \mathbf{u}[n] - \hat{\mathbf{G}}[n]\mathbf{d}[n]. \tag{27}$$

This can be rewritten as

$$\mathbf{e}_{\text{ff}} = \mathbf{E}_G \mathbf{d}[n] + \mathbf{v}[n]. \tag{28}$$

Assuming that the observation noise is independent of the channel estimation error and the transmitted data symbol and that $d[n]$ is a white, unit variance data sequence yields

$$\mathbf{R}_{\mathbf{e}_{\text{ff}}} = \mathbf{R}_{E_G} + \mathbf{R}_v . \tag{29}$$

Thus, subtracting the assumed $\mathbf{R}_v$ from the estimated $\mathbf{R}_{\mathbf{e}_{\text{ff}}}$ yields an estimate of $\mathbf{R}_{E_G}$. Results generated using this method are shown in Sec. VI A.

The second method of estimating $\mathbf{R}_{E_G}$ was to estimate the channel scattering function as described in Appendix C. The scattering function estimates were used to calculate the diagonal elements of $\mathbf{R}_{\epsilon,\epsilon}[1]$ using Eq. (25). The estimate of $\mathbf{R}_{E_G}$ then equals the trace of this matrix times the identity matrix. Recall that this method assumes that the channel fluctuations are well modeled as a WSSUS process and the off-diagonal elements of $\mathbf{R}_{\epsilon,\epsilon}[1]$ therefore equal zero. Results generated using this method are shown in Sec. VI B.

The presentation of the experimental data here serves several purposes. The results in Sec. VI A provide experimental verification of the error expressions derived in Sec.

III and quantify the relative contributions of MAE and excess error to the soft decision error for the conditions encountered. They also offer some insight into the factors that limit equalizer performance which motivates the modification of the CE-DFE presented in Sec. VII. The results in Sec. VI B verify the applicability of Eq. (25) to predicting channel estimation error and is a further step in the development of quantitative expressions for predicting the performance of equalizers given knowledge of environmental conditions. Finally, the results generated using the CE-DFE and P-TR equalizers are compared which quantifies the improvement realized by the MMSE filter coefficient optimization and DFE structure of the CE-DFE when operating with only a small hydrophone array aperture as is the case here.

A. CE-DFE performance prediction from the residual prediction error correlation matrix ($\mathbf{R}_{\mathbf{e}_{\text{ff}}}$)

Figure 5 shows the predicted and observed estimation errors when processing data set 334 with a one channel CE-DFE. There is close agreement between the observed and predicted soft decision error. For this figure, the assumed noise level was σ_{vt}^2. These data show a rough balance between the MAE and excess error. For comparison, the data were also processed with an equalizer that assumed a noise level of σ_{va}^2. The result of this processing showed a 3 dB increase in excess error but a 2.5 dB drop in MAE. Had the channel fluctuations been slower allowing for the estimation of a larger portion of the channel impulse response, this MAE figure would more accurately represent the true MAE for the equalizer. Thus, in this case, the performance of the equalizer is dominated by the excess error, that is the ability to track the channel.

A striking feature of the data in Fig. 5 is the periodic structure of the fluctuations in the error. The minimum soft decision error in each period is between −5 and −6 dB. By comparison, the processing of data set 331 (data collected during relatively calm conditions) yielded a soft decision error of −6.1 dB. This indicates that even in periods of rough surface conditions, the channel cycles periodically between conditions of a high rate of fluctuation and low rate of fluctuation. The time scale of this cyclic behavior matches that of the dominant surface waves measured during this time interval. In addition, the conditions during a low rate of channel fluctuations are close to as good as those encountered during calm surface conditions. This conclusion is further supported by the analysis in Sec. VI B.

Figure 6 shows comparable data for a four channel CE-DFE processing data set 334. Again, there is close agreement between the observed and predicted soft decision error. In this case, the error is dominated by the excess error. A feature of the data present in Fig. 6 and to a certain extent in Fig. 5 is that the periodic nature of the soft decision error is due primarily to fluctuations in the excess error and not the MAE. In fact, the MAE is relatively constant indicating that the MAE is somewhat insensitive to the particular realization of the channel encountered. Figure 7 shows the bit error rates achieved by the one and four channel equalizers.
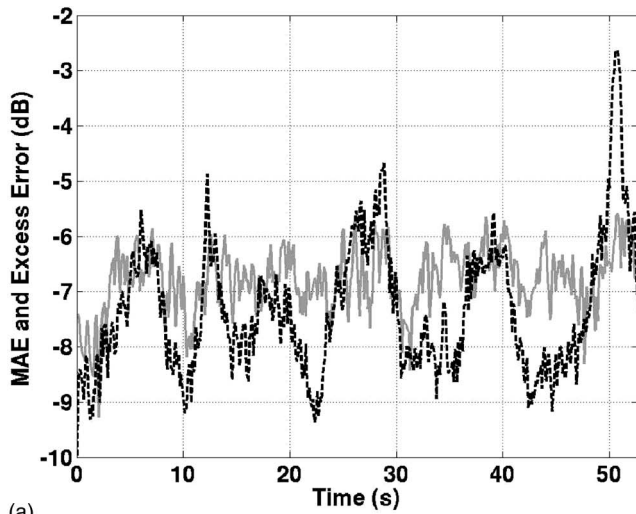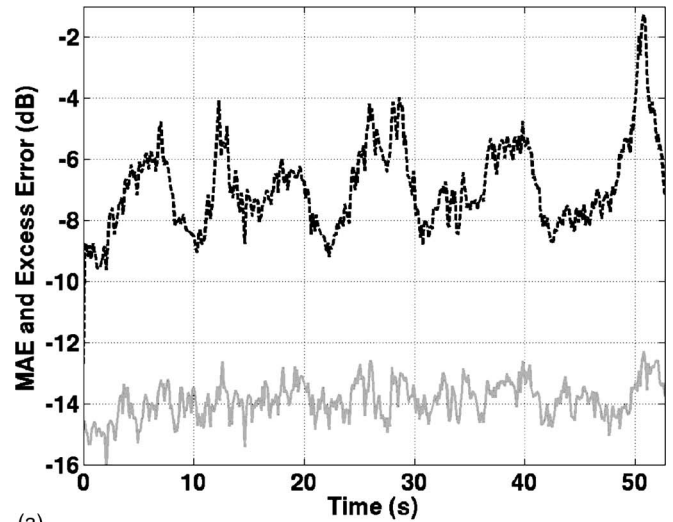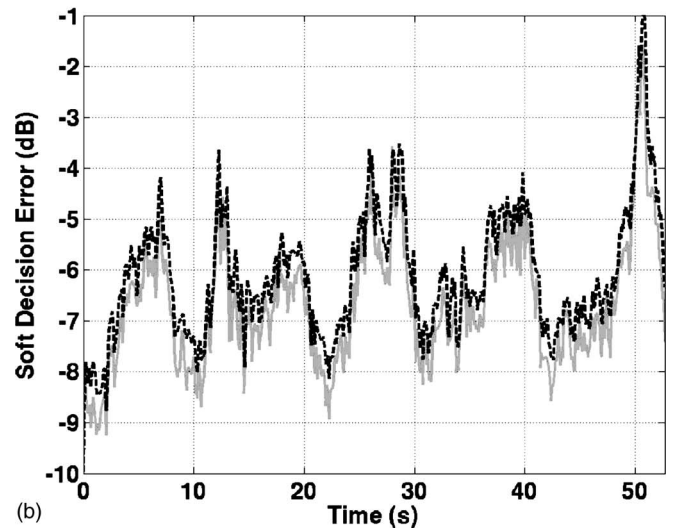
(a)
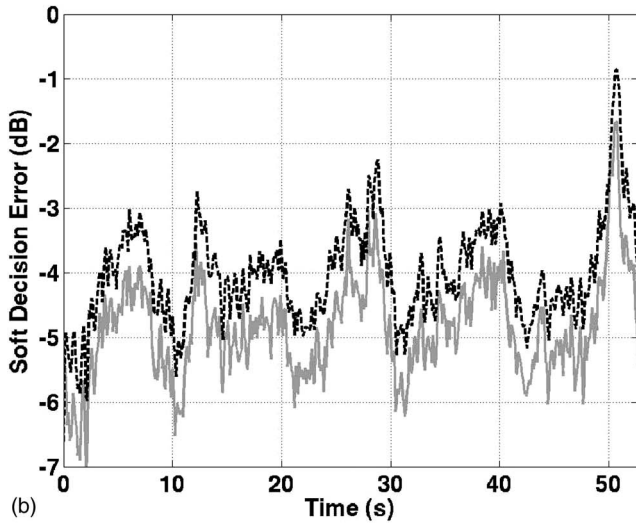
(b)

FIG. 5. The predicted and measured data estimation errors are shown for a one channel CE-DFE processing data set 334. All errors are shown in dB relative to the data symbol variance of $\sigma_d^2 = 1$. (a) The predicted MAE (solid gray line) and excess error (dashed black line). The excess error was calculated using a running average of the full autocorrelation matrix of the feed-forward filter residual prediction error. The average used an exponential weighting with an exponential weighting factor of $\lambda = 0.999$. Note that the levels of the two different errors are commensurate with the excess error exceeding the MAE during times of rapid channel fluctuations and the reverse being the case at times with no rapid channel fluctuations. (b) The predicted (dashed black line) and observed (solid gray line) soft decision errors. The predicted error shown here is the sum of the predicted MAE and excess error shown in (a). Note the periodic nature of the equalizer soft decision error performance. The data in (a) indicate that the primary source of the periodic variability is the excess error. In addition, the periodicity is in line with the dominant surface wave period of 8.5 s that was measured during the time that these data were collected. Note that the predicted soft decision error consistently exceeds the observed error by up to 1 dB.

(a)

(b)

FIG. 6. The predicted and measured data estimation errors are shown for the four channel CE-DFE processing data set 334. All errors are shown in dB relative to the data symbol variance of $\sigma_d^2 = 1$. (a) The predicted MAE (solid gray line) and excess error (dashed black line). The excess error was calculated using a running average of the full autocorrelation matrix of the feed-forward filter residual prediction error. The average used an exponential weighting with an exponential weighting factor of $\lambda = 0.999$. Note that the excess error is slightly greater than that shown in Fig. 5(a) for the one channel CE-DFE while the MAE is significantly less than the MAE for the one channel CE-DFE. The limiting factor in this four channel case is the excess error due to a combination of channel estimation errors and a lack of robustness with respect to such errors rather than the MAE which reflects the static channel structure and the ambient noise. (b) The predicted (dashed black line) and observed (solid gray line) soft decision errors. The predicted error shown here is the sum of the predicted MAE and excess error shown in (a). The data here exhibit the same periodicity as that exhibited by the data shown in Fig. 5.

B. Performance prediction using channel scattering functions and the influence of surface scattering

While the use of the observed residual prediction error correlation matrix to predict equalizer performance is effective for understanding the factors limiting performance in a postexperiment data analysis scenario, it is less valuable for the purposes of predicting system performance ahead of time. The capability to predict communications system per-

formance ahead of time based upon assumed or measured environmental conditions is highly desirable for future work on system trade-off studies or the configuration of communications networks. A step in this direction is to be able to predict performance based upon the channel scattering function. The channel scattering function is sufficient to calculate the diagonal elements of the channel estimation error correlation matrix, $\mathbf{R}_{E_G}$. In some cases, these diagonal elements are adequate to yield accurate predictions of equalizer per-
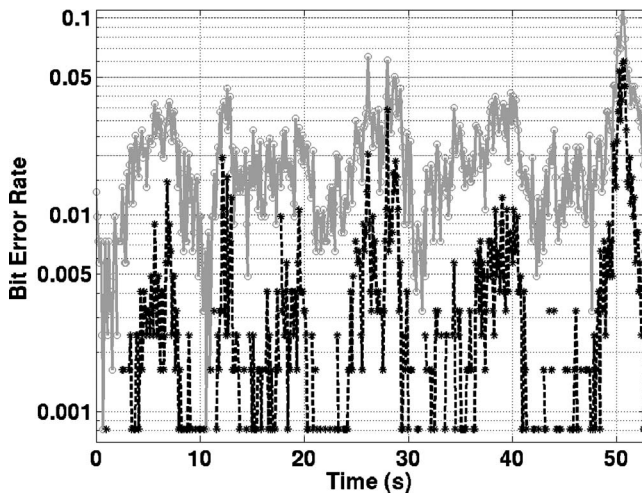
FIG. 7. Bit error rate for the processing of the data set 334 by the one (solid gray line with circles) and four (dashed black line with asterisks) channel CE-DFEs. These bit error rates were calculated over 1230 symbol intervals corresponding to a time interval of 0.1102 s. Thus, the minimum error rate shown is 0.000 81, which corresponds to one demodulation error in a single averaging block. Points in time where successive marks (asterisks for the four channel data) are not connected by lines indicate periods where there were no demodulation errors in a block. The data for both equalizers show periodic increases in bit error rate corresponding to the increases in soft decision error shown in Figs. 5 and 6.

formance. In these cases, a predicted channel scattering function based upon acoustic propagation and scattering models would be the input to the prediction process. In the cases where the diagonal elements of $\mathbf{R}_{E_G}$ are not sufficient to yield accurate performance predictions, additional work needs to be done.

Figure 8 shows the predicted and observed channel and data estimation errors for a one channel CE-DFE processing data set 334 with an estimated noise level of σ_{vt}^2. The predictions in these cases were made using estimates of the channel scattering function and show close agreement with the observed errors. In other cases the agreement was not close. When processing data set 334 with a one channel CE-DFE using an estimated noise level of σ_{va}^2, the predictions of the excess error were 11–16 dB above the values shown in Fig. 5. This resulted in an overprediction of the soft decision error by up to 15 dB. In the case of the four channel CE-DFE processing data set 334, the excess error predictions made using only the diagonal elements of $\mathbf{R}_{E_G}$ resulted in a lower excess error than shown in Fig. 6 and an underprediction of the soft decision error by approximately 2 dB. Thus, additional work needs to be done with respect to predicting the channel estimation error correlation matrix $\mathbf{R}_{E_G}$ from a priori information.

The channel scattering function approach is also useful for determining which channel fluctuations most significantly contribute to the degradation of performance by the equalizers. Figure 9 shows a prediction of the estimation error for each tap of the channel impulse response as a function of time in data set 334. These channel estimation errors are the cause of the degradation of equalizer performance. The data clearly show a periodic structure to the increase in channel estimation errors that results in an increased excess

error, soft decision error, and bit error rate in Figs. 5–8. The errors are largest for the single surface bounce paths reflecting higher energy levels of these arrivals and/or a higher rate of fluctuation for these arrivals.

The errors for the single surface bounce paths are also highly localized in delay and time indicating their dependence on conditions in a fairly localized scattering region of the ocean surface. The single surface bounce path errors in the period of high error in the interval of 25–30 s also show a pattern that is characteristic of the surface wave focusing phenomenon reported in Preisig et al.[11] Interestingly, the increase in excess error during this period shown in Figs. 5 and 6 shows a distinctive double hump that may be a result of this surface wave focusing.

Comparing the high error region around a time of 50 s in Fig. 9 with the expanded view of the channel impulse estimates shown in Fig. 10 confirms that this region corresponds to a high intensity arrival with a rapidly increasing delay. This analysis indicates that a potential area for the improvement of future channel estimate based equalizers is the improvement of techniques for tracking these rapidly moving impulse response arrivals. While the improvement of the ability to estimate the channel impulse response is one approach to improving equalizer performance, another approach is to improve the robustness of these equalizers with respect to channel estimation errors. Such an approach is presented in Sec. VII.

C. Comparison of adaptive channel estimate decision feedback and passive time reversal equalizers

A passive time reversal equalizer was used to process data set 334 using both one and four channels of data. In both cases, the performance of the equalizer is dominated by the MAE. For the one channel case, the MAE was 4.14 dB resulting in a soft decision error of 4.24 dB and a bit error rate of 0.2. For the four channel processing, the MAE was 2.54 dB, the soft decision error was 2.58 dB, and the bit error rate was 0.17. The predicted and observed soft decision errors in both cases showed excellent agreement.

The error of the P-TR equalizer in this case is completely dominated by the MAE despite the observed large errors in estimating the channel impulse response showing in Fig. 8(a). This result is not surprising since the passive time reversal equalizer relies on near orthogonality of the replica vector for the data symbol to be estimated ($\mathbf{g}_o$) and the remaining columns of the channel impulse response matrix ($\mathbf{G}$) in order to achieve interference cancellation. This orthogonality is difficult to achieve with no spatial aperture (the one channel case) or the 18.7 cm aperture available in the four channel case. However, the results shown in Flynn et al.[3] indicate that the performance of passive time reversal systems improves substantially as a significantly wider aperture and more channels of data are available.

VII. ROBUST DECISION FEEDBACK EQUALIZATION USING RESIDUAL PREDICTION ERRORS

The results in Sec. VI show that the excess error resulting from channel estimation errors and the sensitivity of a
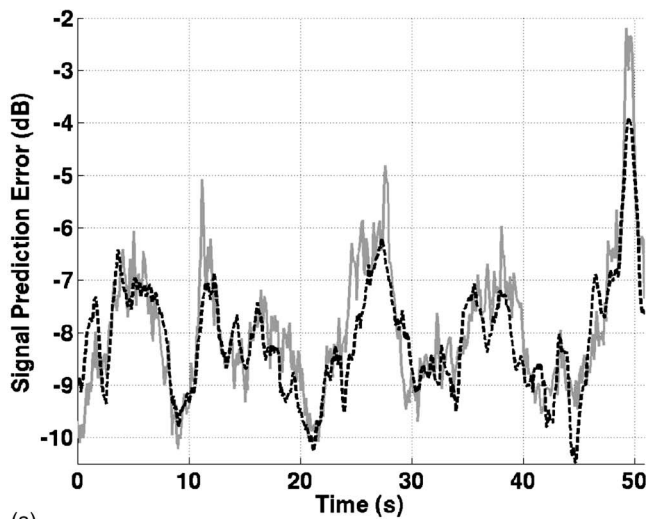
(a)
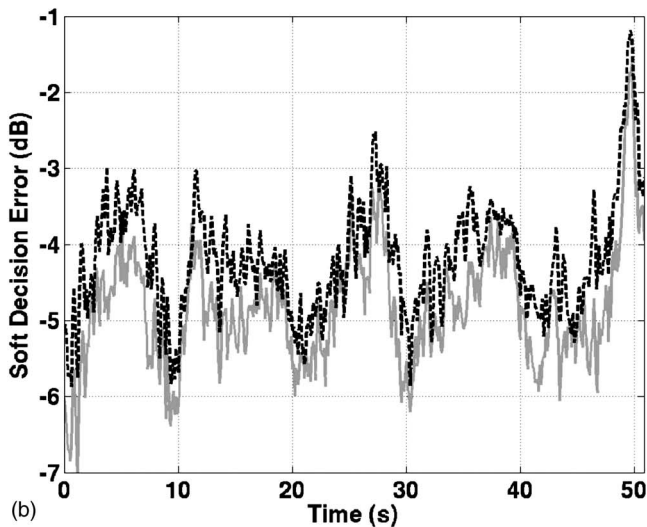
(b)

FIG. 8. Comparison of predicted and observed estimation errors for the channel estimation algorithm and the one channel CE-DFE processing data set 334. (a) The predicted (dashed black line) and observed (solid gray line) received signal residual prediction error achieved by the exponentially weighted least-squares algorithm used to estimate that time-varying channel impulse response as shown in Fig. 1. The errors are shown in dB relative to the mean received signal level over the data set. The channel estimate was updated at the symbol rate of 11 161 symbols/s and the exponential weighting factor was $\lambda = 0.9933$. The prediction of the residual prediction error is calculated using Eq. (25) and equals the trace of the calculated error correlation matrix. Note that in the periods of slow channel fluctuations when the error is low, the predicted error closely matches the observed error. However, the predicted error is significantly below the observed error in times of rapid channel fluctuations. It is believed that this is due to the inability to accurately estimate the channel scattering function during times when the channel is not only changing rapidly but the channel scattering function is changing rapidly as well. Such a situation has been shown to exist in some situations where signals are scattered off of surface gravity waves (Preisig et al.,[11]). The analysis shown in Figs. 9 and 10 indicates that it may exist here as well. (b) The predicted (dashed black line) and observed (solid gray line) soft decision error achieved by the CE-DFE processing data set 334. All errors are shown in dB relative to the data symbol variance of $\sigma_d^2 = 1$. While the predicted and observed errors show close agreement, the predicted error is based upon an underprediction of channel estimation error as evidenced by the data shown in (a). This indicates that the prediction of soft decision error itself overestimates the error as discussed in the text and is consistent with the data shown in Fig. 5(b).
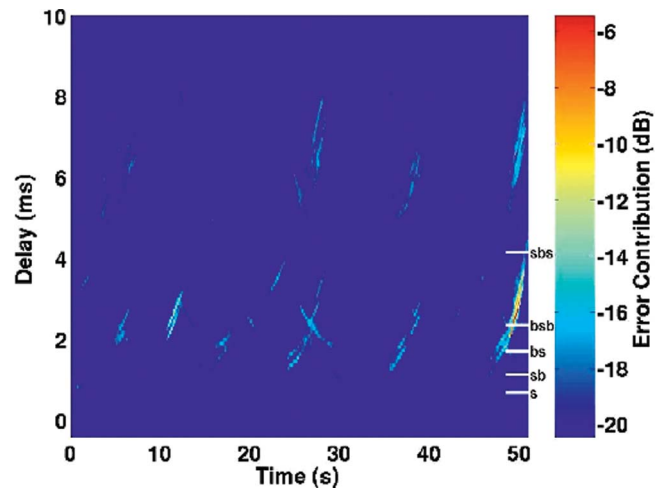

FIG. 9. The predicted estimation error for each tap of the time-varying channel impulse response for the time period corresponding to data set 334. The errors are shown in dB relative to the mean intensity of the direct path arrival. The delay axis has been shifted in the same manner as Figs. 4 and 10 so that a delay of zero corresponds to the peak of the direct path arrival. These predicted errors are calculated based on estimates of the channel scattering function as was the case for the data shown in Fig. 8(a). The white tic marks on the right axis correspond to modeled arrival times for successive propagation paths as described in the caption of Fig. 4. The data clearly show the periodic nature of the increase in channel estimation errors. In addition, the data show moderate coincidence between the time at which the single surface bounce arrivals (the first four arrivals) show high errors and the periods of time at which later arrivals show high error. The most intense sources of error are the single surface bounce arrivals. The coherent steep diagonal structure in the time/delay plane of these errors indicates that they are caused by a single scattered path with a scattering point that is moving rapidly in space resulting in a rapid rate of change of the propagation path length.

traditional CE-DFE to those errors is a major contributor to the overall soft decision error. Thus, a significant performance improvement can be expected by improving the robustness of the CE-DFE with respect to channel estimation
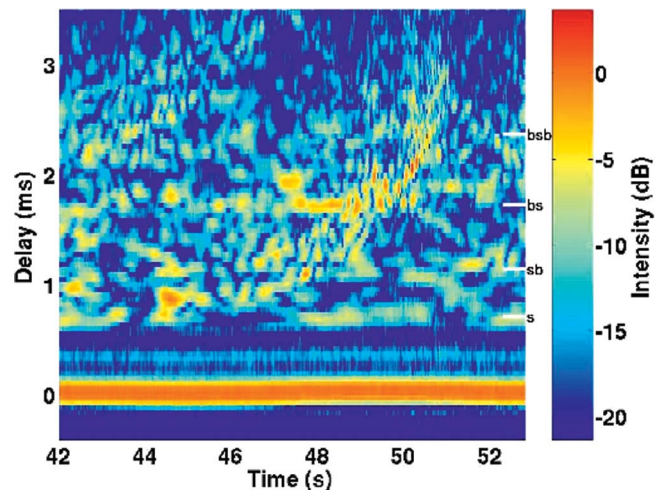

FIG. 10. An expanded view of the intensity of the channel estimates for data set 334 shown in Fig. 4(b). Note the rapid increase in delay of the arrival between the bottom/surface and bottom/surface/bottom marks at around the time of 50 s. The time and delay of this arrival corresponds to the largest source of channel estimation error shown in Fig. 9 and supports the conclusion that the surface scattered arrivals with rapid rates of change of their propagation path lengths comprise a large source of channel estimation error in the data shown here.

errors. The work presented in Stojanovic *et al.*[4] showed that the MMSE CE-DFE equalizer given knowledge of the statistics of the channel estimation errors is one that calculates the filter weights by accounting for these estimation errors in an assumed noise correlation matrix. However, the estimation of the statistics of the channel estimation errors was not addressed.

The residual prediction error of the input signal to the feedforward filter defined in Eq. (27) can be calculated directly by the equalizer and used to estimate the required assumed noise correlation matrix. The equalizer using this approach is referred to here at the residual prediction error DFE (RPE-DFE). The data presented here indicate that this is an effective way of implementing the robust CE-DFE derived in Stojanovic *et al.*[4] and results in a significant performance improvement.

The sample effective noise correlation matrix is this example was calculated as

$$\hat{\mathbf{R}}_{\mathbf{e}_{\mathrm{ff}}}[n] = \sum_{m=0}^{n} \lambda_e^{n-m} \mathbf{e}_{\mathrm{ff}}[m] \mathbf{e}_{\mathrm{ff}}^h[m] \qquad (30)$$

with an exponential weighting factor of $\lambda_e = 0.999$. This effective noise correlation matrix was used in the place of $\mathbf{R}_v$ to estimate the matrix $\mathbf{Q}$ in Eq. (9). The resulting $\mathbf{Q}$ was used in Eq. (10) to calculate the RPE-DFE filter coefficients.

Figure 11 shows the soft decision error and bit error rates achieved by one and four channel RPE-DFEs processing data set 334. The results show the approach improves the robustness of the equalizer but does not completely eliminate the sensitivity to channel estimation errors. A computationally simpler approach was also tried in which $\hat{\mathbf{R}}_{\mathbf{e}_{\mathrm{ff}}}[n]$ was assumed to be the identity matrix times the mean value of the diagonal elements of $\hat{\mathbf{R}}_{\mathbf{e}_{\mathrm{ff}}}[n]$ as defined in Eq. (30). This approach yielded some performance improvement but not nearly as much as that indicated by the data in Fig. 11. This indicates that it is important to properly account for not only the level of the residual prediction error but also the eigenstructure of the residual prediction error correlation matrix.

VIII. CONCLUSIONS

Expressions for predicting the minimal achievable error and excess error of channel estimated based linear and decision feedback equalizers have been derived and analyzed. The analysis of experimental data verifies that the expressions can accurately predict equalizer performance when the second-order statistics of the errors in the channel impulse response estimates are known. The data also show that the excess error was always a significant contributor to the soft decision error when rough sea surface conditions prevailed. This motivates the use of residual prediction errors to estimate an effective noise correlation matrix that results in an improved robustness of the CE-DFE to channel estimation errors. The expressions for the minimal achievable error allow its interpretation in terms of the projection of the replica vector for the data symbol being estimated onto the replica vectors for the interfering data symbols. This lends insight into the very poor minimal achievable error exhibited by the
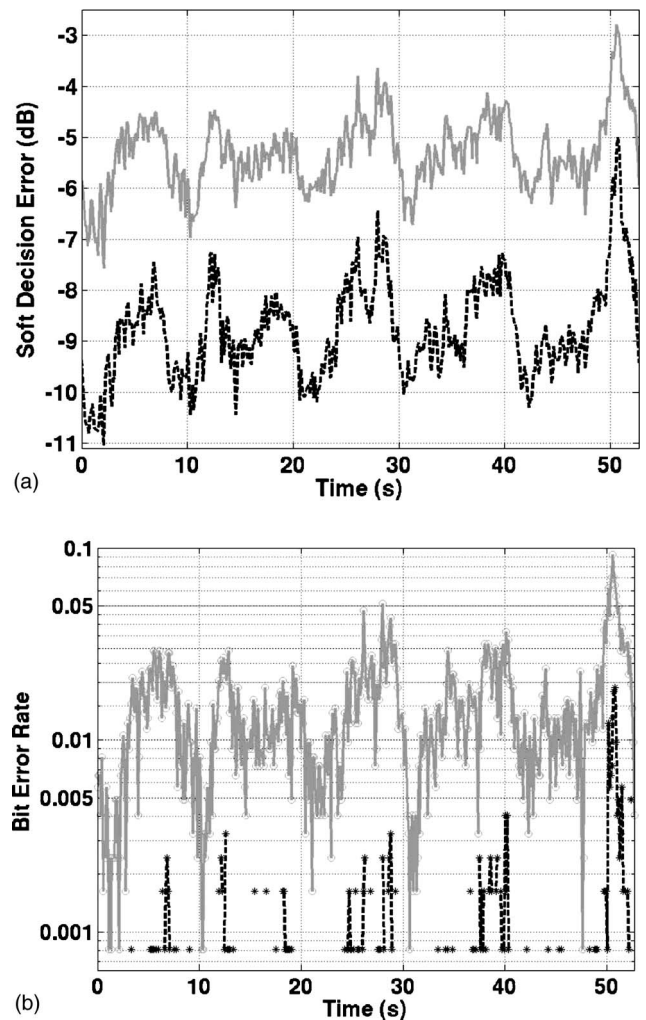

FIG. 11. Estimation error performance with RPE-DFEs processing of data set 334. (a) The soft decision error for the one (solid gray line) and four (dashed black line) channel RPE-DFEs. (b) The bit error rate for the processing achieved the one (solid gray line with circles) and four (dashed black line with asterisks) channel RPE-DFEs. These bit error rates were calculated over 1230 symbol intervals corresponding to a time interval of 0.1102 s. Thus, the minimum error rate shown is 0.000 81, which corresponds to one demodulation error in a single averaging block. Points in time where successive marks (circles for the one channel data, asterisks for the four channel data) are not connected by lines indicate periods where there were no demodulation errors in a block. Note the improvement in performance with respect to the data presented for the standard CE-DFEs in Figs. 5 and 6. This performance improvement is particularly strong in the times when the channel estimation error is poor. This confirms the improvement in equalizer robustness with respect to channel estimation errors afforded by the residual prediction error approach.

P-TR equalizer compared to that exhibited by the CE-DFE when using data from a small array aperture.

An expression relating the channel estimation error for an exponentially weighted least-squares algorithm to the spectral correlation matrix of the channel impulse response is presented. For the case of WSSUS channels, this allows for the prediction of equalizer performance based upon the statistics of the fluctuations of the channel impulse response in the form of the channel scattering function. This is an important step toward the eventual goal of quantitatively predicting equalizer performance based upon predictions or observations of environmental conditions. The analysis of data

James C. Preisig: Robust coherent equalization and performance analysis

from the SPACE02 experiment collected during rough weather conditions shows that the equalizer performance characterized by both the excess error and the soft decision error is periodic with the period related to the wave period. Surprisingly, the equalizer performance during the best times of each period is almost as good as the performance achieved when processing data collected during calm weather conditions. If this feature proves to hold for a broad range of shallow water environments, it may be exploitable to improve the overall data throughput of underwater acoustic communications systems.

Finally, the scattering function analysis approach shows the distribution of channel estimation errors as a function of delay in the channel impulse response. The analysis shows a well-defined structure in delay and time. This structure indicates that the primary contributor to the error is the rate of change of the propagation path length for well-defined single surface bounce arrivals. This motivates future work on improving the ability of channel estimation algorithms to track or estimate these arrivals.

ACKNOWLEDGMENTS

APPENDIX A: DERIVATION OF EQUALIZER COEFFICIENT AND MAE EXPRESSIONS

The derivation of the equalizer coefficients assumes that the estimates of the channel impulse response are accurate (e.g., $\mathbf{G}=\hat{\mathbf{G}}$) and that past symbol decisions are accurate (e.g., $\mathbf{d}_{\mathrm{fb}}[n]=\hat{\mathbf{d}}_{\mathrm{fb}}[n]$). Therefore, the caret is dropped off of the estimates of these quantities throughout this derivation. Starting with the CE-DFE, let

$$\mathbf{z}[n]=\begin{bmatrix}\mathbf{u}[n]\\\mathbf{d}_{\mathrm{fb}}[n]\end{bmatrix}, \tag{A1}$$

and

$$\mathbf{h}=\begin{bmatrix}\mathbf{h}_{\mathrm{ff}}\\\mathbf{h}_{\mathrm{fb}}\end{bmatrix}.$$

Then, from Eq. (5)

$$\hat{d}_s[n]=\mathbf{h}^h\mathbf{z}[n].$$

The equalizer coefficients are the solution to

$$\mathbf{h}_{\mathrm{opt}}=\arg\min_{\mathbf{h}} E[|\mathbf{h}^h\mathbf{z}[n]-d[n]|^2|\mathbf{G}],$$

where the expectation is shown as being conditioned on $\mathbf{G}$. It is straightforward to show that

$$\mathbf{h}_{\mathrm{opt}}=\mathbf{R}_{z,z}^{-1}\mathbf{r}_{z,d}, \tag{A2}$$

and

$$\sigma_{o_{\mathrm{DFE}}}^2=\sigma_d^2-\mathbf{r}_{z,d}^h\mathbf{R}_{z,z}^{-1}\mathbf{r}_{z,d}, \tag{A3}$$

where $\mathbf{R}_{z,z}=E[\mathbf{z}[n]\mathbf{z}^h[n]|\mathbf{G}]$ and $\mathbf{r}_{z,d}=E[\mathbf{z}[n]d^*[n]|\mathbf{G}]$. Recall that $d[n]$ is a unit variance and white sequence and is independent of $v[n]$. Then, substituting Eq. (8) into Eq. (A1)

and using the result to evaluate these expectations yields

$$\mathbf{r}_{z,d}=\begin{bmatrix}\mathbf{g}_0\\\mathbf{0}_{L_{\mathrm{fb}}\times 1}\end{bmatrix}, \tag{A4}$$

and

$$\mathbf{R}_{z,z}=\begin{bmatrix}(\mathbf{g}_0\mathbf{g}_0^h+\mathbf{Q}+\mathbf{G}_{\mathrm{fb}}\mathbf{G}_{\mathrm{fb}}^h) & \mathbf{G}_{\mathrm{fb}}\\\mathbf{G}_{\mathrm{fb}}^h & \mathbf{I}\end{bmatrix}, \tag{A5}$$

where $\mathbf{Q}$ is as defined in Eq. (9). Partition $\mathbf{R}_{z,z}^{-1}$ as follows:

$$\mathbf{R}_{z,z}^{-1}=\begin{bmatrix}\widetilde{\mathbf{A}} & \widetilde{\mathbf{D}}\\\widetilde{\mathbf{C}} & \widetilde{\mathbf{B}}\end{bmatrix},$$

where $\widetilde{\mathbf{A}}$ and $\widetilde{\mathbf{B}}$ are square matrices with sizes L_a+L_c and L_{fb}, respectively. $\widetilde{\mathbf{C}}$ and $\widetilde{\mathbf{D}}$ are appropriately sized rectangular matrices. Then, $\mathbf{h}_{\mathrm{ff}}=\widetilde{\mathbf{A}}\mathbf{g}_0$, $\mathbf{h}_{\mathrm{fb}}=\widetilde{\mathbf{C}}\mathbf{g}_0$, and $\sigma_{o_{\mathrm{DFE}}}^2=1-\mathbf{g}_0^h\widetilde{\mathbf{A}}\mathbf{g}_0$. It can be shown that

$$\widetilde{\mathbf{A}}=(\mathbf{Q}+\mathbf{g}_0\mathbf{g}_0^h)^{-1}=\mathbf{Q}^{-1}-\frac{\mathbf{Q}^{-1}\mathbf{g}_0\mathbf{g}_0^h\mathbf{Q}^{-1}}{1+\mathbf{g}_0^h\mathbf{Q}^{-1}\mathbf{g}_0}, \tag{A6}$$

and

$$\widetilde{\mathbf{C}}=-\mathbf{G}_{\mathrm{fb}}^h\widetilde{\mathbf{A}}. \tag{A7}$$

The first equality in Eq. (A6) and the equality in Eq. (A7) follow from the application of the matrix inversion identity for partitioned matrices (Kailath[12]). The second equality in Eq. (A6) follows from the well-known identity for the inverse of a rank one update to a matrix. Using Eqs. (A6) and (A7) to evaluate the expressions for the CE-DFE filter coefficients and MAE yields

$$\mathbf{h}_{\mathrm{ff}}=\widetilde{\mathbf{A}}\mathbf{g}_0=\frac{\mathbf{Q}^{-1}\mathbf{g}_0}{1+\mathbf{g}_0^h\mathbf{Q}^{-1}\mathbf{g}_0},$$

$$\mathbf{h}_{\mathrm{fb}}=\widetilde{\mathbf{C}}\mathbf{g}_0=-\mathbf{G}_{\mathrm{fb}}^h\mathbf{h}_{\mathrm{ff}},$$

and

$$\sigma_{o_{\mathrm{DFE}}}^2=\frac{1}{1+\mathbf{g}_0^h\mathbf{Q}^{-1}\mathbf{g}_0}.$$

The derivation of similar expressions for the MMSE Linear equalizer starts with $\mathbf{z}[n]=\mathbf{u}[n]$ and $\mathbf{h}=\mathbf{h}_{\mathrm{lin}}$,

$$\mathbf{h}_{\mathrm{opt}}=\mathbf{h}_{\mathrm{lin}}=\mathbf{R}_{z,z}^{-1}\mathbf{r}_{z,d}, \tag{A8}$$

and

$$\sigma_{o_{\mathrm{lin}}}^2=\sigma_d^2-\mathbf{r}_{z,d}^h\mathbf{R}_{z,z}^{-1}\mathbf{r}_{z,d}. \tag{A9}$$

Then,

$$\mathbf{r}_{z,d}=\mathbf{g}_0, \tag{A10}$$

and

$$\mathbf{R}_{z,z}=\mathbf{g}_0\mathbf{g}_0^h+\mathbf{Q}+\mathbf{G}_{\mathrm{fb}}\mathbf{G}_{\mathrm{fb}}^h.$$

Evaluating $\mathbf{R}_{z,z}^{-1}$ yields

$$\mathbf{R}_{\zeta,z}^{-1} = (\mathbf{Q} + \mathbf{G}_{\text{fb}}\mathbf{G}_{\text{fb}}^h)^{-1}$$

$$- \frac{(\mathbf{Q} + \mathbf{G}_{\text{fb}}\mathbf{G}_{\text{fb}}^h)^{-1}\mathbf{g}_0\mathbf{g}_0^h(\mathbf{Q} + \mathbf{G}_{\text{fb}}\mathbf{G}_{\text{fb}}^h)^{-1}}{1 + \mathbf{g}_0^h(\mathbf{Q} + \mathbf{G}_{\text{fb}}\mathbf{G}_{\text{fb}}^h)^{-1}\mathbf{g}_0}. \qquad \text{(A11)}$$

Substituting Eqs. (A10) and (A11) into Eqs. (A8) and (A9) gives

$$\mathbf{h}_{\text{lin}} = \frac{(\mathbf{Q} + \mathbf{G}_{\text{fb}}\mathbf{G}_{\text{fb}}^h)^{-1}\mathbf{g}_0}{1 + \mathbf{g}_0^h(\mathbf{Q} + \mathbf{G}_{\text{fb}}\mathbf{G}_{\text{fb}}^h)^{-1}\mathbf{g}_0},$$

and

$$\sigma_{o_{\text{lin}}}^2 = \frac{1}{1 + \mathbf{g}_0^h(\mathbf{Q} + \mathbf{G}_{\text{fb}}\mathbf{G}_{\text{fb}}^h)^{-1}\mathbf{g}_0}.$$

For the passive time-reversal equalizer, the filter coefficients are the matched filter normalized so that $\mathbf{h}_{\text{tr}}\mathbf{g}_0 = 1$. Therefore $\mathbf{h}_{\text{tr}} = \mathbf{g}_0/\mathbf{g}_0^h\mathbf{g}_0$. This yields a soft decision of

$$\hat{d}_s[n] = \mathbf{h}_{\text{tr}}^h\mathbf{u}[n] = d[n] + \frac{\mathbf{g}_0}{\mathbf{g}_0^h\mathbf{g}_0}(\mathbf{G}_{\text{fb}}\mathbf{d}_{\text{fb}}[n] + (\mathbf{v}[n]$$

$$+ \mathbf{G}_o\mathbf{d}_o[n])),$$

and a soft decision error of

$$\hat{d}_s[n] - d[n] = \frac{\mathbf{g}_0}{\mathbf{g}_0^h\mathbf{g}_0}(\mathbf{G}_{\text{fb}}\mathbf{d}_{\text{fb}}[n] + (\mathbf{v}[n] + \mathbf{G}_o\mathbf{d}_o[n])).$$

Evaluating the expectation of the magnitude squared of this soft decision error yields

$$\sigma_{o_{\text{tr}}}^2 = \frac{\mathbf{g}_0^h(\mathbf{Q} + \mathbf{G}_{\text{fb}}\mathbf{G}_{\text{fb}}^h)\mathbf{g}_0}{(\mathbf{g}_0^h\mathbf{g}_0)^2}.$$

APPENDIX B: DERIVATION OF EQ. (25)

The time-varying channel impulse response, $\widetilde{\mathbf{g}}^h[n]$, is modeled as a zero-mean, wide-sense stationary vector random process with a correlation function

$$\mathbf{R}_{\widetilde{g},\widetilde{g}}[m] \triangleq E[\widetilde{\mathbf{g}}[n]\widetilde{\mathbf{g}}^h[n+m]].$$

The vector $\widetilde{\mathbf{g}}[n]$ has dimension $N_o \times 1$.

The system identification problem is to estimate $\widetilde{\mathbf{g}}[n]$ from observations $u[n]$ where

$$u[n] = \widetilde{\mathbf{g}}^h[n]\mathbf{d}[n] + v[n]. \qquad \text{(B1)}$$

$\mathbf{d}[n]$ is a known zero-mean, white vector time series with $E[\mathbf{d}[n]\mathbf{d}^h[n]] = \mathbf{R}_{d,d}$ and is independent of $\widetilde{\mathbf{g}}[m]$ for all m and n. $v[n]$ is zero-mean, white observation noise with a variance σ_v^2. $v[n]$ is independent of both $\mathbf{d}[m]$ and $\widetilde{\mathbf{g}}[m]$ for all m and n. The estimate is computed as the solution to Eq. (24).

One form of the recursive least-squares solution to Eq. (24) denoted by $\hat{\widetilde{\mathbf{g}}}[n]$ is (Haykin[13])

$$\hat{\widetilde{\mathbf{g}}}[n] = \hat{\widetilde{\mathbf{g}}}[n-1] + \hat{\mathbf{R}}_{d,d}^{-1}[n]\mathbf{d}[n](u[n]-\hat{u}[n])^*, \qquad \text{(B2)}$$

where

$$\hat{u}[n] = \hat{\widetilde{\mathbf{g}}}^h[n-1]\mathbf{d}[n], \qquad \text{(B3)}$$

and $\hat{\mathbf{R}}_{d,d}[n] = \sum_{m=0}^n \lambda^{(n-m)}\mathbf{d}[m]\mathbf{d}^h[m]$. The quantity of interest is the M-step state prediction error,

$$\boldsymbol{\epsilon}[n+M|n] \triangleq \hat{\widetilde{\mathbf{g}}}[n] - \widetilde{\mathbf{g}}[n+M], \qquad \text{(B4)}$$

and its error correlation matrix

$$\mathbf{R}_{\epsilon,\epsilon}[M] \triangleq E[\boldsymbol{\epsilon}[n+M|n]\boldsymbol{\epsilon}^h[n+M|n]].$$

For the case considered here, the value of $M=1$ is used. While a strict evaluation of the expressions for $\mathbf{R}_{E_G} \triangleq E[\mathbf{E}_G\mathbf{E}_G^h|\hat{\mathbf{G}}]$ requires the evaluation of $\mathbf{R}_{\epsilon,\epsilon}[M]$ at multiple lags greater than one, the results achieved using $M=1$ suffice to demonstrate the techniques presented in this paper.

The derivation of the error correlation equations relies on a state space representation of the process $\widetilde{\mathbf{g}}[n]$ as derived in Sec. 1 of Appendix B. The state equation for the estimation error is then derived in Sec. 2 of Appendix B. The state equations for the process and the estimation error are combined in a coupled state model in Sec. 2 a of Appendix B. Sections 2 b and 2 c of Appendix B present the solution of the coupled state equations for required cross-correlation matrices and for $\mathbf{R}_{\epsilon,\epsilon}[1]$.

1. The state space representation of $\widetilde{\mathbf{g}}[n]$

For any matrix correlation function $\mathbf{R}_{\widetilde{g},\widetilde{g}}[m]$ that corresponds to a rational power spectrum, it is possible to define another zero-mean stationary vector random process $\mathbf{g}[n]$ with dimension $N_g \geq N_o$ such that

$$\mathbf{g}[n+1] = \mathbf{A}\mathbf{g}[n] + \mathbf{w}[n], \qquad \text{(B5)}$$

$$\widetilde{\mathbf{g}}[n] = \mathbf{S}_g\mathbf{g}[n] \qquad \text{(B6)}$$

for a selection matrix $\mathbf{S}_g$, [The selection matrix $\mathbf{S}_g$ is an $N_o \times N_g$ matrix with all elements equal to zero except for a single element in each row that equals one], and

$$\mathbf{R}_{\widetilde{g},\widetilde{g}}[m] = \mathbf{S}_g\mathbf{R}_{g,g}[m]\mathbf{S}_g^h \qquad \text{(B7)}$$

is the above-specified matrix correlation function. Here, $\mathbf{A}$ is an $N_g \times N_g$ state transition matrix and $\mathbf{w}[n]$ is zero-mean, white process noise with a correlation matrix $\mathbf{R}_w$. $\mathbf{w}[n]$ is independent of $\mathbf{g}[0]$ for all $n \geq 0$ and is independent of $v[m]$ and $\mathbf{d}[m]$ for all n and m. Note that for $M > 0$,

$$\mathbf{R}_{g,g}[M] = \mathbf{R}_{g,g}[0](\mathbf{A}^M)^h. \qquad \text{(B8)}$$

2. The error state equation

Equations (B5) and (B6) can be manipulated and combined to yield

$$\widetilde{\mathbf{g}}[n+1] = \widetilde{\mathbf{g}}[n] - \mathbf{S}_g(\mathbf{I}-\mathbf{A})\mathbf{g}[n] + \mathbf{S}_g\mathbf{w}[n]. \qquad \text{(B9)}$$

Substituting Eqs. (B1) and (B3) into Eq. (B2) and substituting Eq. (B4) into the result yields

$$\hat{\widetilde{\mathbf{g}}}[n] = \hat{\widetilde{\mathbf{g}}}[n-1] + \hat{\mathbf{R}}_{d,d}^{-1}[n]\mathbf{d}[n](v^*[n] - \mathbf{d}^h[n]\boldsymbol{\epsilon}[n|n$$

$$-1]). \qquad \text{(B10)}$$

Subtracting Eq. (B9) from Eq. (B10), substituting Eq. (B4) into the result, and grouping terms results in the error state equation

James C. Preisig: Robust coherent equalization and performance analysis

$$\boldsymbol{\epsilon}[n+1|n]=(\mathbf{I}-\hat{\mathbf{R}}_{d,d}^{-1}[n]\mathbf{d}[n]\mathbf{d}^h[n])\boldsymbol{\epsilon}[n|n-1]+\mathbf{S}_g(\mathbf{I}$$
$$-\mathbf{A})\mathbf{g}[n]+\hat{\mathbf{R}}_{d,d}^{-1}[n]\mathbf{d}[n]v*[n]-\mathbf{S}_g\mathbf{w}[n].$$
$$(B11)$$

Equation (B11) is a difference equation with a random time-varying state transition matrix, $(\mathbf{I}-\hat{\mathbf{R}}_{d,d}^{-1}[n]\mathbf{d}[n]\mathbf{d}^h[n])$ and coefficient matrix $\hat{\mathbf{R}}_{d,d}^{-1}[n]$. The direct averaging method (Kushner[14]) may be used to evaluate the convergence behavior of this equation in an average sense. Under the assumption that these matrices vary slowly with time (i.e., λ is close to one), they can be replaced by their expected values. The resulting expression can be used to evaluate the steady state behavior of Eq. (B11) in an average sense. Following the convention adopted in Haykin[13] and Eleftheriou *et al.*[15] $\hat{\mathbf{R}}_{d,d}^{-1}[n]$ is replaced by $(1-\lambda)\mathbf{R}_{d,d}^{-1}$ and $\mathbf{d}[n]\mathbf{d}^h[n]$ is replaced by $\mathbf{R}_{d,d}$. With these substitutions, Eq. (B11) can be rewritten as

$$\boldsymbol{\epsilon}[n+1|n]=\lambda\boldsymbol{\epsilon}[n|n-1]+\mathbf{S}_g(\mathbf{I}-\mathbf{A})\mathbf{g}[n]+(1$$
$$-\lambda)\mathbf{R}_{d,d}^{-1}\mathbf{d}[n]v*[n]-\mathbf{S}_g\mathbf{w}[n]. \qquad (B12)$$

a. The coupled state equations

The state equations (B5) and (B12) can be written in coupled form as

$$\begin{bmatrix}\mathbf{g}[n+1]\\\boldsymbol{\epsilon}[n+1|n]\end{bmatrix}=\begin{bmatrix}\mathbf{A}&\mathbf{0}\\\mathbf{S}_g(\mathbf{I}-\mathbf{A})&\lambda\mathbf{I}\end{bmatrix}\begin{bmatrix}\mathbf{g}[n]\\\boldsymbol{\epsilon}[n|n-1]\end{bmatrix}$$
$$+\begin{bmatrix}\mathbf{I}&\mathbf{0}\\-\mathbf{S}_g&(1-\lambda)\mathbf{R}_{d,d}^{-1}\mathbf{d}[n]\end{bmatrix}\begin{bmatrix}\mathbf{w}[n]\\v*[n]\end{bmatrix}.$$
$$(B13)$$

For a stable matrix $\mathbf{A}$ and $0<\lambda<1$, the state transfer matrix in Eq. (B13) is stable and the equation describes a zero-mean stationary random process. Therefore

$$\lim_{n\to\infty}E[\boldsymbol{\epsilon}[n+1|n]]=\mathbf{0}. \qquad (B14)$$

Define

$$\mathbf{R}_{\epsilon,g}[m]\triangleq E[\boldsymbol{\epsilon}[n+1|n]\mathbf{g}^h[n+m]]$$

and let $\mathbf{R}_{g,\epsilon}[m]\triangleq\mathbf{R}_{\epsilon,g}^h[m]$. Then, taking the outer product of both sides of Eq. (B13), taking the expectation of both sides, and taking the limit as $n\to\infty$ yields the following four equations that are satisfied by $\mathbf{R}_{g,g}[0]$, $\mathbf{R}_{\epsilon,g}[1]$, $\mathbf{R}_{g,\epsilon}[1]$, and $\mathbf{R}_{\epsilon,\epsilon}[1]$:

$$\mathbf{R}_{g,g}[0]=\mathbf{A}\mathbf{R}_{g,g}[0]\mathbf{A}^h+\mathbf{R}_w, \qquad (B15)$$

$$\mathbf{R}_{\epsilon,g}[1]=\lambda\mathbf{R}_{\epsilon,g}[1]\mathbf{A}^h+\mathbf{S}_g(\mathbf{I}-\mathbf{A})\mathbf{R}_{g,g}[0]\mathbf{A}^h-\mathbf{S}_g\mathbf{R}_w, \qquad (B16)$$

$$\mathbf{R}_{g,\epsilon}[1]=\lambda\mathbf{A}\mathbf{R}_{g,\epsilon}[1]+\mathbf{A}\mathbf{R}_{g,g}[0](\mathbf{I}-\mathbf{A})^h\mathbf{S}_g^h-\mathbf{R}_w\mathbf{S}_g^h, \qquad (B17)$$

$$\mathbf{R}_{\epsilon,\epsilon}[1]=\lambda^2\mathbf{R}_{\epsilon,\epsilon}[1]+\mathbf{S}_g(\mathbf{I}-\mathbf{A})\mathbf{R}_{g,g}[0](\mathbf{I}-\mathbf{A})^h\mathbf{S}_g^h$$
$$+\lambda\mathbf{R}_{\epsilon,g}[1](\mathbf{I}-\mathbf{A})^h\mathbf{S}_g^h+\lambda\mathbf{S}_g(\mathbf{I}-\mathbf{A})\mathbf{R}_{g,\epsilon}[1]$$
$$+\mathbf{S}_g\mathbf{R}_w\mathbf{S}_g^h+(1-\lambda)^2\sigma_v^2\mathbf{R}_{d,d}^{-1}. \qquad (B18)$$

b. Solving the coupled state equations for R$_{\epsilon,g}$[1] and R$_{g,\epsilon}$[1]

Equation (B16) can be rewritten as

$$\mathbf{R}_{\epsilon,g}[1]=\lambda\mathbf{R}_{\epsilon,g}[1]\mathbf{A}^h+\mathbf{S}_g\mathbf{R}_{g,g}[0]\mathbf{A}^h-\mathbf{S}_g(\mathbf{A}\mathbf{R}_{g,g}[0]\mathbf{A}^h$$
$$+\mathbf{R}_w).$$

Substituting Eq. (B15) into the last term of this equation and rearranging terms yields

$$\mathbf{R}_{\epsilon,g}[1]=\mathbf{S}_g\mathbf{R}_{g,g}[0](\mathbf{A}^h-\mathbf{I})(\mathbf{I}-\lambda\mathbf{A}^h)^{-1}. \qquad (B19)$$

Since $0<\lambda<1$ and the magnitude of each eigenvalue of $\mathbf{A}$ is less than one, the matrix $\lambda\mathbf{A}$ has eigenvalues all of whose magnitudes are less than one. Therefore (Golub *et al.*[16])

$$(\mathbf{I}-\lambda\mathbf{A}^h)^{-1}=\sum_{m=0}^{\infty}\lambda^m(\mathbf{A}^m)^h. \qquad (B20)$$

Substituting Eq. (B20) into Eq. (B19), rearranging terms, and substituting Eq. (B8) into the result yields

$$\mathbf{R}_{\epsilon,g}[1]=-\mathbf{S}_g\left(\sum_{m=0}^{\infty}\lambda^m\mathbf{R}_{g,g}[m]\right)(\mathbf{I}-\mathbf{A}^h). \qquad (B21)$$

Similarly,

$$\mathbf{R}_{g,\epsilon}[1]=-(\mathbf{I}-\mathbf{A})\left(\sum_{m=0}^{\infty}\lambda^m\mathbf{R}_{g,g}^h[m]\right)\mathbf{S}_g^h. \qquad (B22)$$

c. Solving the coupled state equations for R$_{\epsilon,\epsilon}$[1]

Substituting Eqs. (B7), (B8), (B15), (B21), and (B22) into Eq. (B18) and rearranging terms yields

$$\mathbf{R}_{\epsilon,\epsilon}[1]=\frac{2}{(1+\lambda)}\left(\mathbf{R}_{\tilde{g},\tilde{g}}[0]-(1-\lambda)\sum_{m=0}^{\infty}\lambda^m\tilde{\tilde{\mathbf{R}}}_{\tilde{g},\tilde{g}}[m\right.$$
$$\left.+1]\right)+\frac{(1-\lambda)}{(1+\lambda)}\sigma_v^2\mathbf{R}_{d,d}^{-1}. \qquad (B23)$$

3. Frequency domain expressions for R$_{\tilde{g},\tilde{g}}$[1]

Let the function $\lambda_1(m)=\lambda^{-1}\lambda^{|m|}$ when $|m|\geqslant1$ and equal 0 for $m=0$. Then, the lag error term (i.e., the first term) in Eq. (B23) may be rewritten as

$$\mathbf{R}_{\text{lag}}[1]=(1+\lambda)^{-1}\left(2\mathbf{R}_{\tilde{g},\tilde{g}}[0]-(1\right.$$
$$\left.-\lambda)\sum_{m=-\infty}^{\infty}\lambda_1(m)\mathbf{R}_{\tilde{g},\tilde{g}}[m]\right).$$

This can be written in the frequency domain as

$$\mathbf{R}_{\text{lag}}[1]=(1+\lambda)^{-1}\frac{1}{2\pi}\int_{-\pi}^{\pi}(2-(1$$
$$-\lambda)\mathcal{F}(\lambda_1))\mathbf{S}_{\tilde{g},\tilde{g}}(\omega)d\omega, \qquad (B24)$$

where $\mathcal{F}(\lambda_M)$ denotes the Fourier transform of the sequence $\lambda_M(m)$. That is,

$$\mathcal{F}(\lambda_M) = \lambda^{-M} \sum_{|m| \geqslant M} \lambda^{|m|} e^{-j\omega m}$$

$$= \frac{e^{-j\omega M} + e^{j\omega M} - \lambda(e^{-j\omega(M-1)} + e^{j\omega(M-1)})}{|1 - \lambda e^{-j\omega}|^2}.$$

(B25)

Evaluating Eq. (B25) for $M = 1$, substituting the result into Eq. (B24), noting that $|1 - \lambda e^{-j\omega}|^2 = (1 - \lambda e^{-j\omega})(1 - \lambda e^{j\omega})$, and combining and rearranging terms yields

$$\mathbf{R}_{\text{lag}}[1] = \frac{1}{2\pi} \int_{-\pi}^{\pi} \frac{|e^{-j\omega} - 1|^2}{|1 - \lambda e^{-j\omega}|^2} \mathbf{S}_{\tilde{g},\tilde{g}}(\omega) d\omega.$$

(B26)

This result is seen to generalize the result presented in Lin *et al.*,[17] which is applicable only to channels for which the power spectrum of the fluctuations of the channel taps is the same for all taps. Substituting Eq. (B26) for the first term in Eq. (B23) and recalling that it is assumed that $\mathbf{R}_{d,d} = \mathbf{I}$ yields Eq. (25).

APPENDIX C: SCATTERING FUNCTION ESTIMATION

The acoustic signals received from each of the transmissions were processed to yield estimates of the time-varying scattering function of the acoustic channel (See Proakis[6] and VanTrees[7]). The received signals for the maximum length sequence (m-seq) transmissions (see Sec. V) were modulated to baseband, low-pass filtered, and then downsampled to a rate of two samples per symbol. The channel scattering function was estimated by matched filtering resampled segments of the received baseband signal with a sequence consisting of frequency shifted versions of three repetitions of the transmitted 4095 point m-seq. The resampling of the baseband signal was necessary to account for the fact that the bandwidth of the transmitted signal was too large to allow for modeling the impact of the rate of change of the length of individual propagation paths as a simple frequency (Doppler) shift. Note that the wideband nature of the signal and rate of change of the propagation path lengths results in a violation of the wide-sense stationary channel assumption. However, the framework of the channel scattering function when evaluation over short time intervals is still useful for quantifying and providing insight into the impact of channel fluctuations on the performance of underwater acoustic communications algorithms.

[1] M. Stojanovic, L. Freitag, and M. Johnson, "Channel-estimation-based adaptive equalization of underwater acoustic signals," in Proceedings of the IEEE Oceans'99 Conference, Seattle, WA, 1999, pp. 985–990.

[2] D. Rouseff, D. R. Jackson, W. L. J. Fox, C. D. Jones, J. A. Ritcey, and D. R. Dowling, "Underwater acoustic communications by pasive phase conjugation: Theory and experimental results," IEEE J. Ocean. Eng. **26**, 821–831 (2001).

[3] J. Flynn, J. A. Ritcey, D. Rouseff, and W. L. J. Fox, "Multichannel equalization by decision-directed passive phase conjugation: Experimental results," IEEE J. Ocean. Eng. **29**, 824–836 (2004).

[4] M. Stojanovic, J. Proakis, and J. Catapovic, "Analysis of the impact of channel estimation errors on the performance of a decision-feedback equalizer in fading multipath channels," IEEE Trans. Commun. **COM-43**, 877–886 (1995).

[5] J. Preisig, "The impact of underwater acoustic channel structure and dynamics on the performance of adaptive coherent equalizers," in *High Frequency Ocean Acoustics*, edited by M. Porter, M. Siderius, and W. Kuperman (American Institute of Physics, New York, 2004), pp. 57–64.

[6] J. G. Proakis, *Digital Communications*, 3rd ed. (McGraw-Hill, New York, 1995), Chaps. 13 and 14, pp. 724–729.

[7] H. L. Van Trees, *Detection, Estimation, and Modulation Theory, Part III* (Wiley Inter-Science, New York, 2001), Chap. 13.

[8] Physical underwater acoustic channels are all causal. However, it is sometimes conceptually convenient to think of some point in delay (the variable *m*) within the impulse response to be the zero delay tap and those points that preceed this point in the delay variable to be acausal taps.

[9] The feedback filter does not need to continuously span the range of past data estimates from $(n-1)$ to $(n - L_{\text{fb}})$. Such feedback filters are said to be "sparse." The modifications to the expressions developed here to handle sparse equalizers are trivial and the conclusions of the analysis are unchanged.

[10] The assumption of unit variance can be made without any loss of generality of the results.

[11] J. Preisig and G. Deane, "Surface wave focusing and acoustic communications in the surf zone," J. Acoust. Soc. Am. **116**, 2067–2080 (2004).

[12] T. Kailath, *Linear Systems* (Prentice-Hall, Englewood Cliffs, NJ, 1980), pp. 656.

[13] S. Haykin, *Adaptive Filter Theory*, 3rd ed. (Prentice-Hall, Upper Saddle River, NJ, 1996).

[14] H. J. Kushner, *Approximation and Weak Convergence Methods for Random Processes With Applications to Stochastic System Theory* (MIT Press, Cambridge, MA, 1984).

[15] E. Eleftheriou and D. Falconer, "Tracking properties and steady-state performance of RLS adaptive filter algorithms," IEEE Trans. Acoust., Speech, Signal Process. **34**, 1097–1109 (1986).

[16] G. H. Golub and C. F. Van Loan, *Matrix Computations*, 3rd ed. (Johns Hopkins University Press, Baltimore, MD, 1996), pp. 58.

[17] J. Lin, J. Proakis, F. Ling, and H. Lev-Ari, "Optimal tracking of time-varying channels: A frequency domain approach for known and new algorithms," IEEE Trans. Selected Areas in Communications **13**, 141–153 (1995).